Efficiency and sustainability of gravel augmentation to restore large regulated rivers: Insights from three experiments on the Rhine River (France/Germany)

Valentin Chardon, Laurent Schmitt, Fanny Arnaud, Hervé Piégay, Anne Clutier

Efficiency and sustainability of gravel augmentation to restore large regulated rivers: insights from three experiments on the Rhine River (France/Germany)

Valentin Chardon[1,2], Laurent Schmitt[1], Fanny Arnaud[2], Hervé Piégay[2], Anne Clutier[3]

1. CNRS UMR 7362 LIVE, University of Strasbourg, Strasbourg, France

2. CNRS UMR 5600 EVS, University of Lyon/Site ENS, Lyon, France

3. Electricité de France, Centre d'Ingénierie Hydraulique (CIH) – Le Bourget-du-Lac, France

Correspondence to: Valentin Chardon, CNRS UMR 7362 LIVE & 5600 UMR 5600, University of Strasbourg, 3 rue de l'Argonne 67000 Strasbourg cedex, France.

E-mail: valentin.chardon@live-cnrs.unistra.fr. Telephone number: +33 3 68 85 09 76

Highlights

- Erosion of stockpile deposits (SDs) is highly dependent on local hydraulic conditions and sediment grain size
- A high channel morphological diversity downstream of gravel augmentations (GAs) increases their positive effects in terms of habitat improvement
- The effects of GAs are transitory due to the downstream transfer of the sediment wave in the absence of an upstream sediment supply
- The feedback from the 3 experiments allows us to formulate operational guidelines and management scenario fostering the efficiency and sustainability of GA operations

Abbreviations

- Cross-section diversity index: CSD
- Gravel augmentation: GA
- Kilometric Point: KP

- Maximal Velocity Ratio: MVR
- Regierungspräsidium Freiburg: RPF
- Stockpile Deposit: SD
- Suitability Index Ratio: SIR

Abstract

Over the last two centuries, rivers were strongly regulated, inducing notable sediment starvation and flow reduction. This regulation altered aquatic habitats, biocenosis and ecosystem services. Gravel augmentation (GA) is increasingly promoted to restore bedload transport, rejuvenate bed sediments and diversify aquatic and riverine habitats. However, practical questions remain in terms of efficiency and sustainability. The objective of this study is to provide feedback from three GA experiments conducted along the Rhine River downstream of the Kembs dam (France/Germany). The restored sites were monitored over a time period from 1 to 7 years according to the sites so that the stockpile deposits (SDs) and channel responses were compared to highlight the strengths and limitations of such experiments. The monitoring was based on topo-bathymetry, bedload tracking and grain size surveys. Two-dimensional hydraulic modeling was also performed to link the SD erosional patterns to critical flow conditions. We show that (i) SD erosion is dependent on the grain size of the introduced sediments and the local flow velocities, (ii) sediment dispersion occurred mostly along the thalweg and increased over time, with a progressive decrease in the virtual velocities, (iii) bathymetric simplification and bed grain-size fining were observed when the downstream sediment diffusion began, but (iv) at mid-term (~ 5 years) local channel diversifications occurred due to the fragmentation of the sediment waves with deposition occurring preferentially on riffles, and (v) new sediment starvation conditions

appeared when the sediment waves travelled downstream in the absence of an upstream sediment supply. The results allow us to propose operational recommendations and management scenario to improve both the efficiency and the sustainability of GAs conducted in large regulated rivers.

Key-words: Gravel augmentation, Restoration, Large rivers, Geomorphic monitoring, Feedbacks, Operational guidelines

1. Introduction

Numerous large rivers have been strongly affected by regulation (Kondolf et al., 2014). Damming is one of the most common infrastructures affecting both water and sediment fluxes, and it often generates sediment starvation below the dams (Kondolf 1997; Wheaton et al., 2004; Petts and Gurnell 2005; Magilligan and Nislow 2005). These conditions cause severe and irreversible geomorphic alterations, such as bed incision, bed armoring and active channel narrowing, which disturb both aquatic and riverine habitats and impair ecosystem services (Kondolf, 1997; Cooper et al., 2017). Moreover, dams accumulate sediments, reducing the reservoir capacities and their life span (Kondolf et al., 2014). Several management strategies were tested to improve the transparency of dams and partially restore downstream bedload transport. These strategies include permanent remediation solutions, such as sediment bypass and sediment pass-through (Sumi et al., 2004). Mechanical excavation of reservoirs and downstream sediment releases have also been used (Kondolf et al., 2014). Dams are also removed, as in the USA where 1,100 dams have been removed in small to moderate watersheds (10 to 1000 km^2) since the 1970s (Foley et al., 2017). Alternative measures consist of mitigating sediment starvation below dams, e.g., by reactivating bank erosion after removing riprap protection (Staentzel et al., 2018a),

reactivating old side channels, remobilizing sediments stored in floodplains (Landon, 2008; Thorel et al., 2018), and implementing gravel augmentations (GAs) (Kondolf et al., 2014; Ock et al., 2013).

GA is becoming a common practice because it provides rapid geomorphic improvement by diversifying bedforms, grain size, and flow conditions (Wheaton et al., 2004.a). First, GAs were conducted in the USA during the 1960s in the form of an ambitious program for fish spawning rehabilitation along 13 dammed rivers in California (Kondolf and Matthews, 1991; Pasternack et al., 2004). In some cases, the GAs were combined with the mechanical creation of in-channel geomorphic features, such as riffles (Pasternack et al., 2004; Ock et al., 2015). Between 1968 and 2000, 316,000 m^3 of sediments were introduced for a total cost of $3,000,000 (Rollet 2007). More recently, GAs were also implemented below 15 Japanese dams (Sumi et al., 2004; Ock et al., 2013). In Europe, the first GAs were realized in 1978 on the Rhine River below the Iffezheim dam (yearly mean volume of 170,000 m^3) to counteract bed incision and maintain a stable water level for navigation (CHR, 2009). GAs were also employed on gravel-bed alpine rivers (Brousse et al., 2018; Heckmann et al., 2017), boulder-bed steep reaches (Downs et al., 2016) and large regulated rivers (Schälchli et al., 2010; Klösch, 2011; Arnaud et al., 2017). Ock et al. (2013) noted several strategies employed to inject sediment into rivers as in-channel bed stockpile, high-flow stockpile, point bar stockpile and high-flow direct injection.

The restoration of fluvial macroforms by GA improves river ecological quality and functionalities. For example, Ock et al. (2015) showed on the Trinity River that in-channel bar development following GA enhanced hyporheic fluxes. Zeug et al. (2013) showed on the Lower American River that both salmon and trout populations increased following GA due to

an increase in spawning areas. Staentzel et al. (2018b) showed that the taxonomic richness of macroinvertebrates increased after a GA experimental operation on the Rhine. Geomorphic assessment of GA is generally carried out over short-term periods (1 to 3 years) and usually focuses on channel topo-bathymetric changes and sediment mobility (Table 1). Grain size diversification and fining are expected, but the results are infrequent because measuring underwater grain size is still challenging. On the other hand, field studies and modeling approaches evaluating the critical conditions for eroding the stockpile deposit (SD) are needed to improve such restoration practices. Numerical modeling studies have shown that various geomorphic responses can be obtained depending on the SD geometric configuration (Battisacco et al., 2016; Juez et al., 2016). This was recently validated in the field by Stähly et al. (2019). To optimize the channel response to GA, additional insights into channel grain size, SD location and geometry and local hydraulic conditions are needed. Implementing a GA operation is not risk-free. Gaeuman et al., 2017 presented three different modes of sediment pulses which are dispersion, translation/dispersion and fragmentation.

In case of sediment translation, large amounts of sediment may travel quickly and impact navigable reaches downstream of the bypassed reaches. Moreover, bedload transport reactivation may destabilize the armor layer (Koll et al., 2010) and bank protections (Arnaud et al., 2017). The proper hydrological functioning of floodplain excavations along incised rivers for flood retention purposes may also be disturbed by bed elevation changes.

The aim of this paper is to present a comparative analysis of three GAs based on short/mid-term (from 2009 to 2017) geomorphic monitoring conducted on a bypassed reach of the Rhine River downstream of the Kembs dam (France/Germany). The objectives are to (i) define the best hydraulic conditions to erode, and therefore remobilize rapidly, the SD, (ii)

evaluate channel responses in terms of sediment mobility, morphodynamics and bed grain size as well as the corresponding temporal scales of these evolutions, (iii) perform a risk analysis to avoid any negative impacts on human and management issues such as bed incision, navigation and flood retention, to consolidate some preliminary results of Arnaud et al. (2017), and (iv) provide some operational guidelines and management scenario for enhancing efficiency and sustainability of GA-based restorations of large rivers.

	Monitoring framework					Hydraulic modeling	Monitored compartments				
Authors	Before/ after protocol	No impacted /impacted protocol	Reach length monitored (m)	Number of post-GA surveys	Duration (year)	Flow conditions for SD erosion	Bedload mobility	Channel topography/ bathymetry	Grain size	Groundwater exchanges	Flow conditions
Rempel and Church 2009	•		~ 2500	3	3			•	•		
Klösch, 2011		•	1110	3	1		•	•			•
Gaeuman, 2013	•		560	1 to 4	4		•	•	•		
Gaeuman, 2014	•		>1000	1	1	•(1)		•			
Ock et al., 2015	•		~ 2000	1	2					•	
Downs et al., 2016		•	>250	2	1		•				
Arnaud et al., 2017	•			4	4		•	•			
Gaeuman et al., 2017	•		>1000	4	1		•	•	•		
Heckmann et al., 2017	•		~ 2000	2	7			•			
Ståhly et al., 2019	•		~ 300	1	< 1		•				•
This study	•		5000 to 12000	1 to 5	1-7	•	•	•	•		

Table 1: Characteristics of some GA monitoring sites. (1) corresponds to a predictive model (SRH-2D) to design SDs.

2. Materials and methods

2.1 Study sites

The Rhine River is the third largest river in Europe, with a drainage basin of 185 000 km² and a river course of 1250 km long. The Upper Rhine, located between Basel and Bingen-am-Rhein, exhibits a nivo-glacial hydrological regime (Figure 1.a; Schmitt et al., 2018). The mean annual discharge is 1059 m^3/s at the Basel gauging station (Wantzen et al., 2019). In this riffle-pool reach, the Rhine is bypassed by the 50 km-long “Grand Canal d’Alsace” (GCA)

between the Kembs diversion dam and Breisach-am-Rhein (Figure 1.b). The minimum flow into this bypassed reach varies between 52 $m^3.s^{-1}$ (winter) and 150 $m^3.s^{-1}$ (spring-summer) in relation to the flow requirements for aquatic and riparian communities (Garnier and Barillier, 2015). Spills occur when the Rhine discharge exceeds 1400 $m^3.s^{-1}$ at Basel gauging station, which corresponds to the maximal capacity of the GCA power plants (Figure 1). This discharge was exceeded an average of 69 days per year between 1932 and 2011 (Arnaud et al., 2015a). This Rhine section exhibits poor ecological functionalities due to severe geomorphological alterations induced by successive engineering works: damming and bypassing, as well as channelization and construction of groin fields since the 19th century (Piégay et al., 2011). Channelization and groin fields induced bed incision, bed armoring and floodplain and side channel disconnection, whereas damming increased active channel narrowing and bedform simplification due to a reduction in morphogenic discharges without any upstream sediment supply (Arnaud et al., 2019).

Since 2010, three GAs have been performed in the first 10 km of the Old Rhine (Figure 1.b) to restore bedload transport, promote bed grain size diversification and increase the heterogeneity of the channel bathymetry to enhance the ecological functionalities of the Old Rhine. The GAs were implemented following the point bar SD method (Ock et al., 2013). In October 2010, a first experimental GA, named Interreg, was achieved within an Interreg program. A SD was implemented within a concave bend and separated from the right bank (Arnaud et al., 2017). Within the framework of the Kembs dam relicensing, Kembs I1 and Kembs I2 GAs (Figure 1.c-d-e) were achieved by Électricité de France in March-April 2015 and March-April 2016, respectively (Garnier and Barillier, 2015). The SDs were located in convex locations. The Kembs I1 SD was connected to the left bank, whereas the Kembs I2 SD was separated between 5 and 10 m from the left bank. The sediments were extracted from

158 the floodplain close to the SD injection areas. The SD volumes equal to 23 000 m^3, 13 000 m^3
159 and 30 000 m^3 (Table 2). These volumes were consistent with the mean annual bedload
160 transport capacity estimated to be 23,000 $m^3.yr^{-1}$ for this part of the reach (El Kadi
161 Abderrezzak, 2009). The critical discharge for bedload entrainment Q_c was estimated to be
162 550 $m^3.s^{-1}$ (El Kadi Abderrezzak, 2009).

SD	Implementation	KP (km)	Volume (m^3)	Length (m)	Width (m)	Height (m)	Mean D_{50}	Mean D_{95}	D_{95}/D_{50}
Interreg	October 2010	182.4 – 183.1	23,000	620	11.00 – 15.00	2.00 - 3.50	35.00	100.60	3.28
Kembs I1	March - April 2015	174.10 -174.525	13,000	425	10.00 - 40.00	2.00 - 3.50	28.00	181.00	6.40
Kembs I2	March - April 2016	176.20 -176.66	30,000	460	15.00 – 40.00	2.00 - 4.50	18.50	105.00	5.95

163 Table 2: Characteristics of the three GAs performed on the Old Rhine. See Section 2.2.4 for
164 details on grain size measurements. The sorting coefficient was based on (Inman 1952).

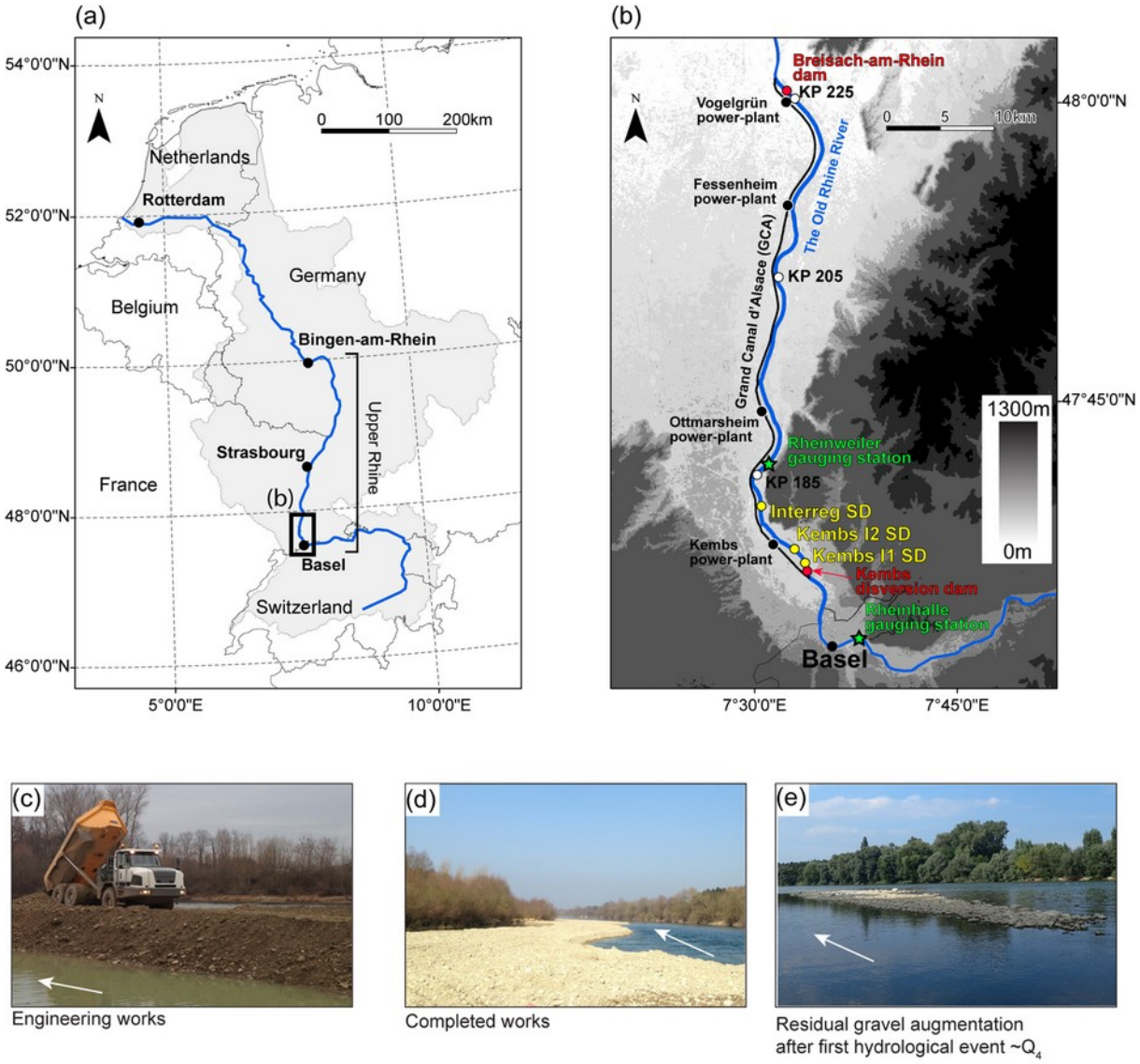

165

166 Figure 1: (a) Location of the Old Rhine river in the Rhine Basin, (b) location of the river
167 network, the hydraulic structures, the gauging stations and the 3 GAs performed along the
168 studied reach, (c) Kembs I2 SD in progress, (d) Kembs I2 SD completed and (e) residual
169 Kembs I2 SD after a Q_4 flood in May 2016. White arrows indicate the flow direction.

170 **2.2 Data collection**

171 2.2.1 Monitoring framework

172 Geomorphic monitoring was applied for each GA at two spatial scales: (i) the SD and (ii) the
173 downstream channel reach, extending 4 to 12 km long depending on the sites. The

monitoring followed a before-after temporal framework that lasted two, three and seven years on Kembs I2, Kembs I1 and Interreg GAs, respectively, corresponding to three, four and seven monitoring periods (Figure 2). The beginnings and ends of each Period P_i correspond to the S_{i-1} and S_i Survey dates, respectively. For each GA, P_0 is the period before the implementation of the SD, and P_{0bis} is the period after the SD implementation and before the first floods. The following P_i are a series of periods following this first flood. Between one and three significant hydrological events occurred for each of these periods, and the flood intensity ranged from Q_1 (1080 $m^3.s^{-1}$) to Q_{15} (2480 $m^3.s^{-1}$). The monitoring methods combined topo-bathymetric surveys, grain size surveys, sediment tracking and two-dimensional hydraulic modeling. The Interreg monitoring presented in this paper (P_5 ¿ is in continuity of the work of Arnaud et al. (2017), who characterized periods P_0 to P_4.

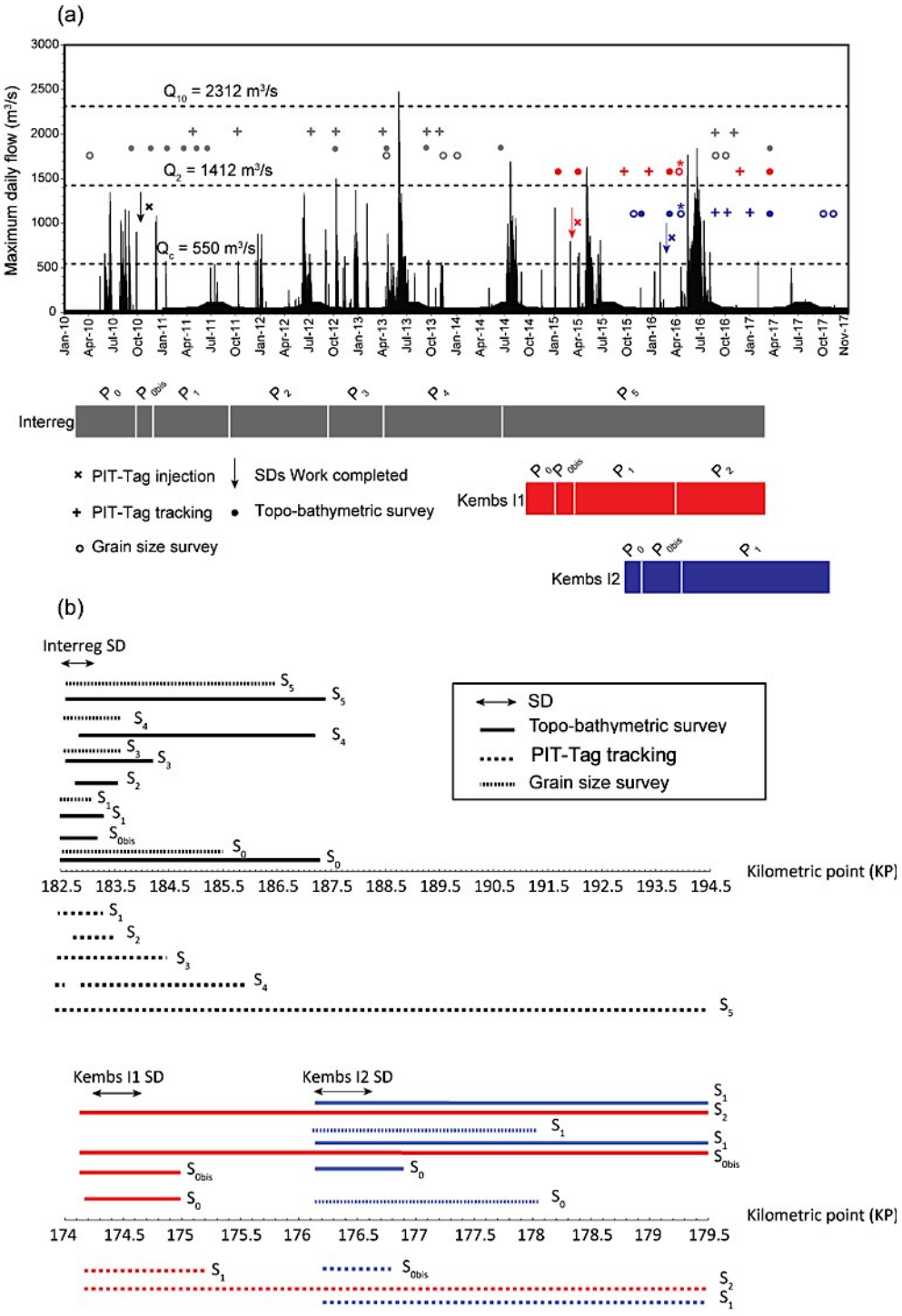

Figure 2: (a) Temporal monitoring framework related to the maximum daily flow in the Old Rhine, obtained by subtracting 1400 $m^3.s^{-1}$ from the discharge at the Basel gauging station and (b) spatial monitoring framework. In (a) circles with a star indicate the volumetric samplings conducted on the SDs. S_x indicates the Survey date and P_x the monitoring Period between two surveys. See Table 3 for details on topo-bathymetric surveys.

2.2.2 Topo-bathymetric surveys

Topo-bathymetric surveys were conducted to assess accurately: (i) the erosion of SDs after first floods and (ii) the habitat diversification along the reaches located downstream the SDs. For Kembs I1 and Kembs I2, S_0 was surveyed in February 2015 and November 2015, respectively, based on cross-section profiles at 5 to 50 m-spaced intervals using a Tritech PA500 single beam echo-sounder (Table 3). An airborne topo-bathymetric LiDAR survey was performed on Kembs I1 in March 2015 ($S_{0\,bis}$), followed by another survey in March 2016 that covered both Kembs I1 (S_1) and Kembs I2 ($S_{0\,bis}$) (Figure 2; Table 3). Another survey in March 2017 covered Kembs I1 (S_2), Kembs I2 (S_1) and Interreg (S_5). All LiDAR surveys were performed at flight elevations close to 400 m using the Optec Titan sensor and during low water turbidity. The spot size was estimated to 0.08-0.12 m in above-water areas and 0.20 m in underwater conditions. The resolution of the LiDAR surveys ranged between 20 and 40 pts/m² for emerged areas and 5 to 10 pts/m² in underwater conditions, depending on the water depth. Due to a sensor malfunction in March 2015, no data were recorded in underwater areas deeper than one meter for this survey. We estimated that about 70 % of the submerged bed area was deeper than 1 m**.** For above-water surfaces the range of mean error was equal to -0.032m to 0.044m and the mean root mean square error was equal to 0.042m for the three airborne topo-bathymetric surveys. During the survey of March 2016, five cross-section profiles were performed simultaneously to control the accuracy of bathymetric data (see table 3). The range of mean error was estimated to -0.086m to +0.083m and the root mean square error equal to 0.083m.".

GA	Survey	Methods	Characteristics	Equipment
Interreg	S_0 *to* S_4	DGPS and single beam echo-sounder	Topo-bathymetric cross-sections (spaced interval equal to 50 m)	Tritech PA500
Interreg	S_5	Topo-bathymetric LiDAR	Full topography (10 to 40 pts/m^2)	Optec Titan sensor
Kembs I1	S_0	DGPS and single beam echo-sounder	Topo-bathymetric cross-sections (spaced interval equal to 5 to 50 m)	Tritech PA500
Kembs I1	S_{0bis}	Topo-bathymetric LiDAR	Full topography (10 to 40 pts/m^2)	Optec Titan sensor
Kembs I1	S_1	Topo-bathymetric LiDAR	Full topography (10 to 40 pts/m^2)	Optec Titan sensor
Kembs I1	S_2	Topo-bathymetric LiDAR	Full topography (10 to 40 pts/m^2)	Optec Titan sensor
Kembs I2	S_0	DGPS and single beam echo-sounder	Topo-bathymetric cross-sections (spaced interval equal to 5 to 50 m)	Tritech PA500
Kembs I2	S_{0bis}	Topo-bathymetric LiDAR	Full topography (10 to 40 pts/m^2)	Optec Titan sensor
Kembs I2	S_1	Topo-bathymetric LiDAR	Full topography (10 to 40 pts/m^2)	Optec Titan sensor

Table 3 : Characteristics of topo-bathymetric surveys achieved in this study.

2.2.3 PIT-tags monitoring

We equipped particles with Passive Integrated Transponders (PIT-tags) to achieve several purposes: (i) evaluate the erosion of SDs according to flow conditions and particle grain size, and (ii) characterize the sediment mobility (travel distances and virtual velocities) and the mode of sediment pulse (dispersion, translation, fragmentation) along the three downstream reaches. We used 23-mm PIT tags for the Interreg GA, a combination of 23-mm and 32-mm tags for Kembs I1, and 32-mm tags for Kembs I2. The PIT tags were developed by Texas Instrument Enterprise and have a maximum vertical reading range of 0.95 m (Arnaud, et al., 2015). For Interreg, bedload tracers were equally distributed between the three principal grain size classes, whereas the tracer grain size distributions (GSD) correspond to the GSD of a gravel bar near Kembs for Kembs I1 and Kembs I2. The PIT tags were placed during S_{0bis} following various injection protocols depending on the GA (Table 4). Each

individual tracer and tracer cluster was geopositioned with a global positioning system Trimble GeoXT 6000 (XY accuracy = 0.1 m).

GA	Period placement	No. of placed tracers	D_{50} of tracers (mm)	Deployment protocols
Interreg	November 2010	1489	71	(i) 19 clusters of 50 tracers placed along 7 cross-sections spaced at 100 m intervals, and (ii) individual tracers deployed along 30 cross-sections spaced at 20 m intervals
Kembs I1	April 2015	1482	53	(i) 10 areas were placed every 50 m comprising 80 to 100 tracers, which were placed individually every meter, and (ii) 13 clusters of 50 tracers deposited in the channel at the toe of the right bank of the SD
Kembs I2	March 2016	1500	54	(i) tracers placed individually at each meter at the surface of the SD along cross sections spaced at 2 m intervals, one tracer was placed in the channel at the toe of the SD on both sides of the SD, and (ii) 16 clusters of 10 to 50 tracers spaced at 100 m intervals, placed in the channel at the toe of the SD on both sides

Table 4 : Characteristics of bedload tracer placed for each GA.

For each bedload tracking survey, the tracers were detected using an antenna connected to a reader system developed by CIPAM Corporation. For emerged and water areas less than 0.6 m deep, a 0.46 m-diameter loop antenna was used, and the tracer IDs were manually recorded with the GPS. In water areas deeper than 0.6 m, a rectangular antenna 1.2 m wide was pulled by boat in the downstream direction, and the same GPS was used in tracking mode (continuously recording each second) to map the tracked areas and determine the position of each detected tracer by synchronizing the on-board GPS and the chronometer. The accuracy of the tracer location was estimated to be 2 m in emerged conditions and water conditions less than 0.6 m while the accuracy was estimated to 5 m in water areas deeper than 0.6 m.

246 2.2.4 Grain size monitoring

247 We performed volumetric samplings to measure the grain size of the injected sediments
248 which composed Kembs I1 (n=2; S_1) and Kembs I2 (n=2; S_{0bis}) SDs. We sampled a minimum
249 mass of sediment according to the grain size of the surface layer, following the equation
250 proposed by Church et al., (1987):

$$mmw = 2{,}882 * Dmax - 47{,}6 \quad (1)$$

251 where mmw corresponds to the minimum mass weight and D_{max} the mean diameter of the
252 30 coarsest particles of the surface layer.
253 For the Interreg SD (S_0), volumetric sampling was performed in the floodplain sediment
254 excavation area (Dittrich et al., 2010). In addition, surface changes in bed grain size were
255 evaluated after the first morphogenic flood (S_1) on the three emerged residual SDs using the
256 Wolman (1954) technique, to evaluate if a coarser surface layer has been developed, which
257 may reduce the residual SD erodibility by the subsequent floods. Moreover, surface grain
258 size changes were also evaluated along the downstream reaches, in both emerged and
259 underwater (water depth < 0.6 m) areas of the active channel, to verify if the GAs diversified
260 and lowered the grain size distributions. For the Interreg downstream reach, the grain size
261 sampling in S_5 (n=414) followed the same protocol as Arnaud (2012), who characterized S_0
262 (n=310), S_3 (n=192) and S_4 (n=143): random sampling of 10 particles at each node of
263 quadrats (10 x 10 m). The surface sampled in S_0, S_3, S_4 and S_5 is equal to 14, 8, 6 and 14% of
264 the monitoring reach, respectively. These relatively low sampled surfaces are explained by
265 the water level which exceeded 0.6 m in the major part of the monitoring reach (> 80%). For
266 Kembs I1 and I2 downstream reaches, an underwater photosieving protocol was applied
267 along transects spaced at 60 m intervals, with sampling points spaced at 5 - 10 m intervals.
268 This photosieving strategy was adopted because the water depth exceeded 1 m in most of

the study areas and reached 4 m locally. For S_0 at Kembs I2, the data collection (n=240) was performed by diving and using a GoPro Hero4+ camera with a constant height equal to 0.52 m. For S_1, high definition (1080p) subaquatic films were obtained along the same transects, by using an Olympus TG-4 camera placed perpendicularly on an aluminum telescopic bar, all deployed from a boat. A rule was placed at the bottom of the telescopic bar to determine the pixel size. Digital images (n=324) were extracted from the subaquatic films using VirtualDub software v.1.10.4. Chardon et al. (2020) showed the capacity of photosieving in underwater conditions to quantify bed grain size. Fisheye deformation on all photos was corrected by using a correction algorithm with Photoshop software. Photos were then cropped to eliminate the corners impacted by the correction. We digitized the ten largest particles in each photograph and calculated the D_{50}, as this metric is close to the D_{95} of the total apparent particles on each photography. Indeed, Houbrechts et al. (2011) demonstrated the advantage to use the mean diameter of ten largest particles to estimate the D_{95} of the grain size distributions. We assumed that this metric is sensitive to bed grain size fining.

2.2.5 Two-dimensional hydraulic modeling

We evaluated the local hydraulic conditions at the SDs by performing two-dimensional hydraulic unsteady flow modeling to compare the intensity of the erosional processes between them. We used the HEC-RAS v.5.0.3 software between the Kembs dam (KP 174.00) and the Rheinweiler gauging station (KP 186.2), which is located 4 km downstream of the Interreg GA (Figure 1). The model contains 146 619 mesh cells with an average cell area of 16 m². The digital elevation model (DEM) used is based on the airborne topo-bathymetric LiDAR of March 2017 because it included a detailed topography of the channel for the entire study reach. The geometries of the three SDs measured in S_{0bis} were integrated into the

DEM. Water levels and instantaneous discharges recorded at the Rheinweiler gauging station during the flood event between May and June 2017 (time step = 15 min) were used as downstream boundary conditions because these discharges ranged between 52 and 2000 $m^3.s^{-1}$, which included the peak discharge of periods P_1 for the three SDs (Figure 2). We assumed that no significant discharges were provided by tributaries along the modeling reach . Only a small tributary is present, the Kander River, for which the 100-year flood is estimated to 56.4 $m^3.s^{-1}$ (information from the RPF). Thus, information from the Rheinweiler gauging station were also used as upstream boundary conditions. The Manning's coefficients implemented in the model are close to those calculated by Béraud (2012) and equal to 0.035 for the active channel and 0.066 for the vegetation areas on the groin fields. Modeling output provided the maximal flow velocities for the peak discharges that occurred during periods P_1 for the three SDs.

2.3 Data processing and analysis

2.3.1 Morphological changes in the SDs

DEMs were produced from point clouds obtained by the airborne topo-bathymetric LiDAR and the terrestrial topo-bathymetric cross-sections datasets conducted along Kembs I1 and Kembs I2 using the 3D Analyst toolbox of ArcMap v.10.3 (cell size = 0.5 m). Cross sections spaced at 25 m intervals were extracted from the DEMs using the ETGeoWizards add-on to calculate the surface eroded on each SD and related to the modelled flow conditions. For the Interreg SD, surface eroded were directly calculated from topo-bathymetric cross-sections (Arnaud et al., 2017). We calculated for each profile the section area at *Si* (in m^2):

$$Section\ area_{(S_i)} = \sum_{i=1}^{n} ¿(x_{i+1} - x_i¿) \vee ¿\left(\frac{Z_{i+1} + Z_i}{2}\right)¿ \quad (2)$$

where x_i and x_{i+1} are the lateral positions and Z_i, and Z_{i+1} are the elevations of successive points (m). n defines the number of points. The reference used to calculate the section area was the toe at the left bank of the SD at S_0.

From the previous equation, we estimated the resulting eroded surface for each cross-section for each SD (in m^2) between two surveys:

$$Eroded\ surface_{S_i \to S_{i+1}} = Section\ area_{(S_{i+1})} - Section\ area_{(S_i)} \quad (3)$$

We estimated the elevation changes uncertainties between S_{0bis} and S_x for Kembs I1 and Kembs I2 SDs by estimating the combined elevation change errors of two paired DEMs from airborne topo-bathymetric LiDAR and according to the equation of Brasington, Langham, and Rumsby (2003):

$$\sigma_{diff} = \sqrt{(\theta¿¿S_i)^2 + (\theta¿¿S_{i+1})^2 ¿¿} \quad (4)$$

where θ_{S_i} and $\theta_{S_{i+1}}$ are the estimated registration errors at S_i and S_{i+1}, respectively. The estimated registration error was estimated to 0.1 m on the Z-axis for all surveys.

Following Bennett et al. (2012), a statistical t-test was performed to identify significant elevation changes for Kembs I1 and Kembs I2 SDs, between two paired DEMs from airborne topo-bathymetric LiDAR and for a given, when $|t|>1$, corresponding to 66% confidence interval:

$$t = \frac{Z_{S_{i+1}} - Z_{S_i}}{\sigma_{diff}} \quad (5)$$

Where Z_{S_i} and $Z_{S_{i+1}}$ are the mean elevation of the DEM cell at S_i and S_{i+1}. From this equation, the elevation changes smaller than σ_{diff} were considered uncertain and not integrated in the analysis of elevation changes (Bennett et al., 2012) but also for sediment budgets.

333 We calculated the sediment budgets for the Kembs I1 and Kembs I2 SDs from the DEM of
334 Differences (DoD):

$$\Delta V_{S_i \to S_{i+1}} = \sum_{i=1}^{n} A * \left(Z_{S_{i+1}} - Z_{S_i} \right) \quad (6)$$

335 where A is the area of the DEM cell, and Z_{S_i} and $Z_{S_{i+1}}$ are the mean elevations of the DEM cell
336 at S_i and S_{i+1}, respectively.
337 We estimated the volume errors for Kembs I1 and Kembs I2 SDs following the equation
338 developed by (Lane et al., 2003):

$$\sigma_v = d^2 . \sqrt{n} . \sigma_{diff} \quad (7)$$

339 where d is the cell size of the DEM (m) and n is the number of cells in each area of
340 signification elevation changes identified by the statistical t-test. For Interreg SD, see Arnaud
341 et al. (2017) for the method used to calculate both the sediment budget and the volume
342 errors.

343 2.3.2 Suitable areas to implement SDs

344 We identified suitable areas in terms of best hydraulic conditions to implement future SDs in
345 order to minimize deposit fixation because the success of GA is dependent on SD erosion.
346 This study was performed for frequent peak flood equal to the Q_2 (1417 $m^3.s^{-1}$). We
347 developed a suitability index ratio (SIR) for each 500 m length of the active channel and
348 calculated as follows:

$$Suitability\ Index\ Ratio = \frac{Area\ of\ flow\ velocity \geq 2.5\, m.s^{-1}}{Area\ of\ active\ channel} \quad (8)$$

We used a flow velocity threshold equal to 2.5 m.s^{-1} because it was found to be the minimal velocity to erode significantly the SDs (see section 3.1.3).

2.3.3 Tracer mobility analysis

We evaluated the mean tracer cloud travel distance for each period P_i using the tracer cloud centroid metric $CP_{(Si)}$ (Piégay et al., 2016; Arnaud et al., 2017):

$$CP_{(Si)} = \frac{\sum_{i=1}^{nrecovered} X_i}{n_{recovered}} \quad (9)$$

where Xi is the longitudinal position (in m) of each tracer linearly referenced along the active channel centerline. For Interreg, the first 12 m of the SD were excluded from the analysis because the tracers do not move. For Kembs I1, tracers detected in the residual SD were not integrated into the calculation of the tracer cloud centroid metric. For each period P_i, the travel distance of the tracer cloud centroid (in m) was calculated as follows:

$$L_{cp} = CP_{(Si+1)} - CP_{(Si)} \quad (10)$$

Then, we calculated the virtual velocity (in m.s^{-1}) for each period P_i by using the travel distance of the tracer cloud centroid:

$$V_{pi} = \frac{L_{CP}}{t_{\geq Q_c}} \quad (11)$$

where $t_{\geq Q_c}$ is the time during which the discharge is greater than or equal to Qc (Church and Hassan, 1992). To calculate this time duration, we used the instantaneous discharge estimated at the Basel gauging station every 10 min and compared it to Q_c.

In order to study the relation between the sediment mobility and the flow competence, we used the two metrics calculated for each period P_i as follows:

(i) The excess unit stream power:

$$\omega_{p_{(i)}} = \frac{\rho_w g (Q_p - Q_c) S}{W} \quad (12)$$

where ρ_w is the water density (kg.m^{-3}), g is the acceleration due to gravity (m.s^{-2}), Q_p is the maximum peak discharge (m^3.s^{-1}), Q_c is the critical discharge (m^3.s^{-1}), S is the average local bed slope (m.m^{-1}) estimated from topo-bathymetric surveys, and W is the mean active channel width (m).

(ii) The cumulative excess stream energy (Schneider et al., 2014) which assess the excess stream energy for an entire period P_i:

$$\sum (\omega_{(t)} - \omega_c) \quad (13)$$

where $\omega_{(t)}$ is the stream energy for a discharge value greater than the critical discharge and $\omega_{(c)}$ is the stream energy for the critical discharge value. (J.m^{-2}). As the time-step measurement at the Basel gauging station is 10 min, we multiplied the excess stream energy by 600 s to calculate all excess stream energy of the period time between two discharges measurements and cumulated all values for the entire period P_i.

In order to identify partial or full bedload mobility, we calculated the mean dimensionless travel distance of the tracer cloud centroid for each grain size class as follows:

$$\text{Mean dimensionless travel distance } ¿ \frac{L_i}{L_{d50}} \quad (14)$$

where L_i is equal to the mean travel distance of the tracer cloud centroid for each grain size class of the recovered tracers, and L_{d50} is the mean travel distance of the median grain size class of the recovered tracers for each survey.

2.3.4 Channel geometry diversification analysis

The evolution of the channel geometry in response to GA operations was assessed using the cross-section diversity index (CSD) developed by Gostner et al. (2013) from topo-bathymetric cross sections along the downstream channel reaches:

$$CSD = \frac{\sum_{i=2}^{n} |\Delta Z_i|}{\sum_{i=1}^{n-1} Y_i} \quad (15)$$

with

$$|\Delta Z_i| = Z_{i-1} - Z_i \quad (16)$$

$|\Delta Z_i|$ is the absolute elevation difference between two consecutive points on a cross section and Y_i is the distance between them. The CSD calculation for Kembs I1 and Kembs I2 in S_0 was based on cross sections surveyed by the RPF in 2009 (not indicated in Figure 2) because the LiDAR surveys of 2015 were only extended 200 m downstream from the two SD sites (Figure 2.b). We also used topo-bathymetric datasets for the period 1985/93-2009 provided by the RPF to compare the CSD of GAs with longer-term changes in the Old Rhine.

3. Results

3.1 Monitoring of the stockpile deposits

3.1.1 Grain size comparison and evolution

The D_{50} calculated from the volumetric samples in S_{0bis} was globally similar for the Interreg and Kembs I1 SDs, and lower for the Kembs I2 SD (Table 2). Regarding the D_{95}, introduced sediments were coarser for Kembs I1 than for the two other SDs. The range of the S_1/S_{0bis} D_{50} ratio was 1.36 to 2.67, 0.45 to 1.27 and equal to 2.35 for Kembs I1, Interreg and Kembs I2, respectively. The surface grain size of the upstream and downstream parts of the Kembs I1 residual SD was very close to the coarse surface layer GSD of a historical gravel bar located at KP 178.2 (D84 = 90.5 mm), indicating partial mobility conditions (Figure 3.b). For Interreg and Kembs I2, no coarse layer was appeared comparatively with the surface GSD of the historical gravel bar (Figure 3.a).

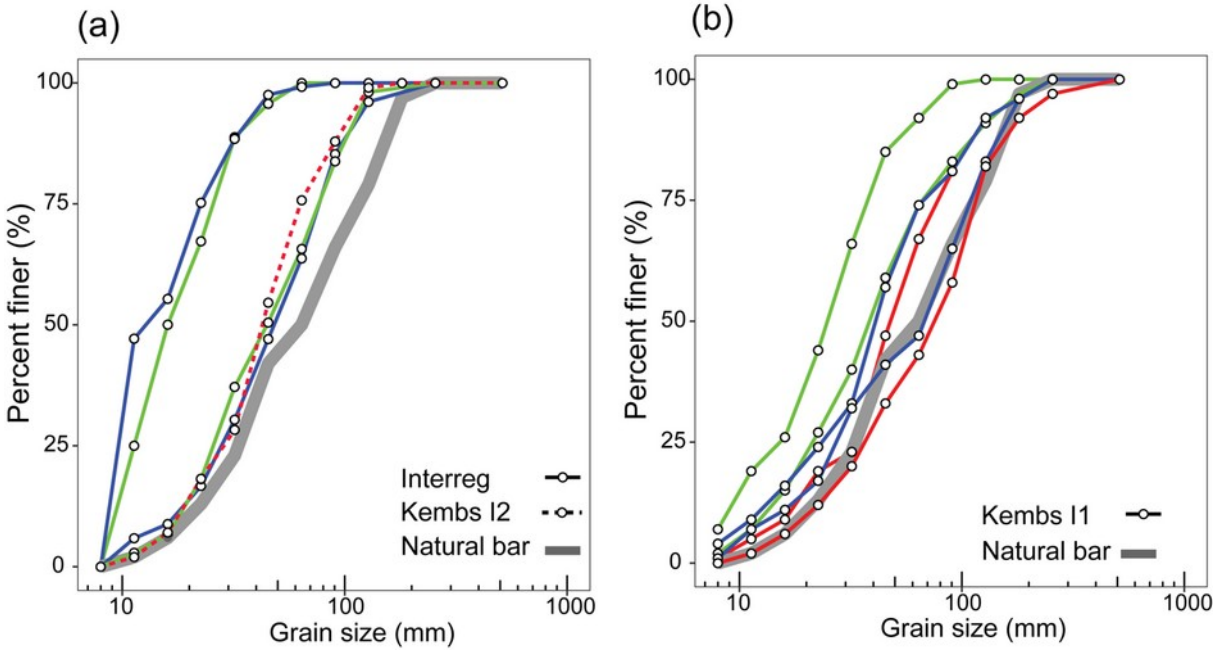

Figure 3: Surface grain size of the three residual SDs in S_1 (a) for Interreg (n=4) and Kembs I2 (n=1), and (b) for Kembs I1 (n=6). Gray lines indicate the surface grain size of a gravel bar

409 located between the Kembs I2 and Interreg SDs (KP 178.2). Blue, green and red colors
410 indicate the upstream, middle and downstream parts of the SDs, respectively.

411 3.1.2 Morphological evolutions and sediment balance comparison

412 We studied both morphological changes and sediment balances of each SD to identify
413 erosion processes. We found statistically significant differences in morphological changes
414 between the three SDs during P_1 (ANOVA-test, p-value = 2e-16. Fewer morphological
415 changes occurred for Kembs I1 (μ=-0.19 m ± 0.28 m) compared to changes for Kembs I2 (μ=-
416 1.05 m ± 0.68 m) and Interreg (μ=-1.12 m ± 0.53 m) (Figure 4.a-c). Sediment budgets were
417 equal to -793.00 m^3 (±12.00 m^3), -15,600 m^3 (±10.00 m^3) and -11,250 m^3 (±199.00 m^3) for
418 Kembs I1, Kembs I2 and Interreg, respectively. These eroded volumes correspond to 6%, 55%
419 and 48% of the initial SD volumes. Two erosional processes occurred for Kembs I2 and
420 Interreg: a toe erosion and a mass failure of the stockpile (Figure 4.e-f). For Kembs I1, only
421 toe erosion occurred (Figure 4.d). The cumulative eroded volumes during P_2 were equal to
422 12% and 95% of the initial SD volumes for Kembs I1 and Interreg, respectively.

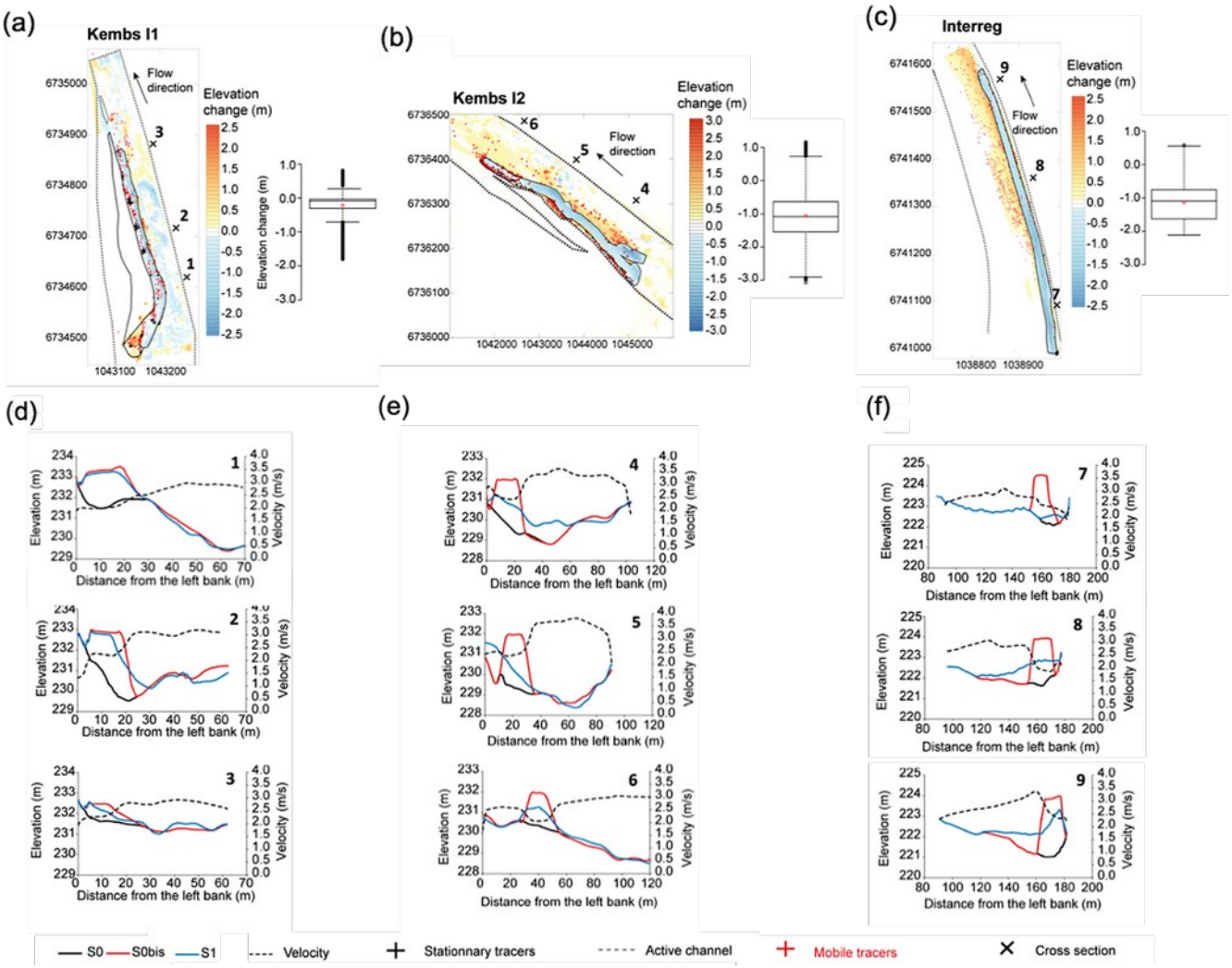

Figure 4: (a) to (c) DEM of differences from S_{0bis} to S_1 for the Kembs I1, Kembs I2 and Interreg SDs, with the location of mobile (red) and stationary tracers (black). Boxplots correspond to the elevation changes along each SD surface from S_{0bis} to S_1. Intervals correspond to the 25th and 75th percentiles, and the lower and upper whiskers correspond to 1.5 times the interval quartile range. Black lines correspond to the median values, and the red points correspond to the mean values. (d) to (f) three cross sections extracted from DoD (cross symbol on (a) to (c)) illustrate the morphological changes for each SD from S_0 to S_1.

3.1.3 Relations between flow conditions and morphological changes of the SDs

We explain the significant differences of the eroded volumes of the SDs due to significative differences on local hydraulic conditions. Statistically significant differences in modeled flow

velocities were found between the three SDs during P_1 (ANOVA-test, P-value = 2e-16). Velocities were lower for Kembs I1 (μ=2.06 m.s^{-1} ± 0.24 m.s^{-1}) compared to those for Interreg (μ=2.20 m.s^{-1} ± 0.26 m.s^{-1}) and Kembs I2 (μ=2.52 m.s^{-1} ± 0.41 m.s^{-1}). A statistically significant relation at the 95% confidence level exists between the eroded areas and the maximum velocity areas calculated on each cross section (R^2 = 0.63; P-value = 4.9e-10; Figure 5.a). Using the maximum velocity as a proxy of the measured eroded areas, the root mean square error (RMSE) and the mean absolute error (MAE) between the predicted eroded areas and the measured eroded areas were equal to 5.37 m^2 and 4.31 m^2, respectively (Figure 5.b).

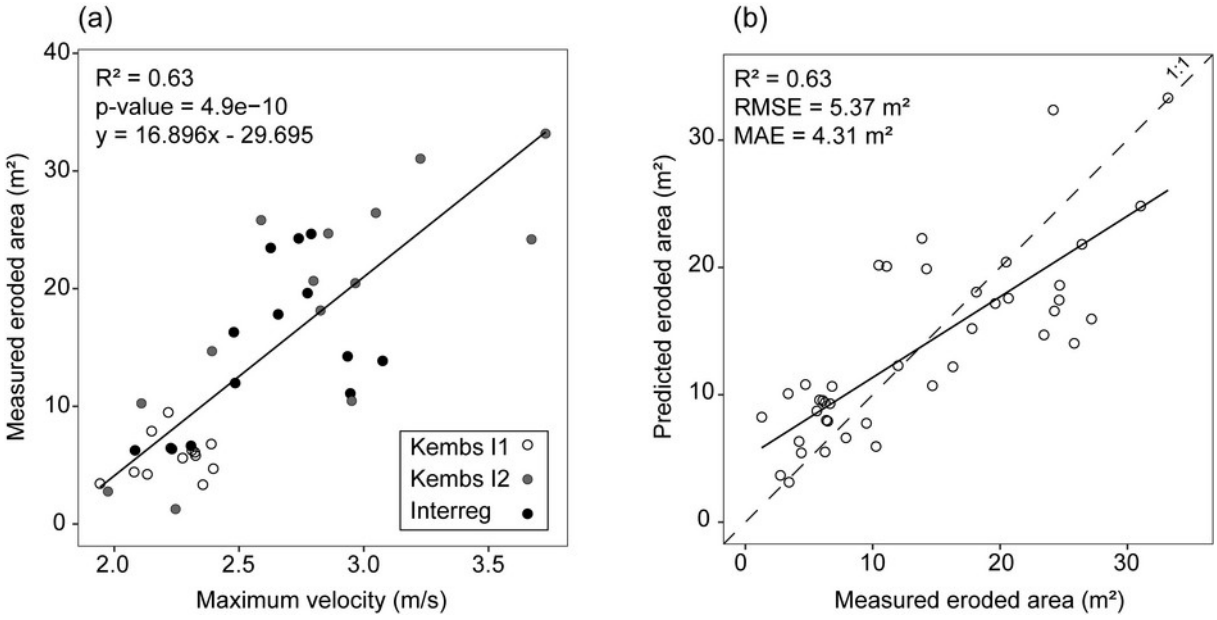

Figure 5: (a) Measured eroded areas according to the maximum velocity calculated for peak floods during P_1 along each SD, and (b) predicted eroded areas by maximal velocities compared with the measured eroded area (m^2). The dashed line corresponds to the 1:1 line.

The recovery rates of the tracers tracked in S_1 were equal to 42%, 33% and 43% for Kembs I1, Kembs I2 and Interreg, respectively. For all SDs, the percentage of mobile tracers ranged from 68% to 87%. Based on logistic regressions, we observed that the tracer movement probability is linked to the flow velocity (P-value < 0.0001). Partial tracer mobility occurred

by flow velocities lower than 2.5 m.s^{-1} with a much lower mobility for the coarsest fraction (128-181 mm). A quasi-full mobility was observed for higher velocities (Figure 6).

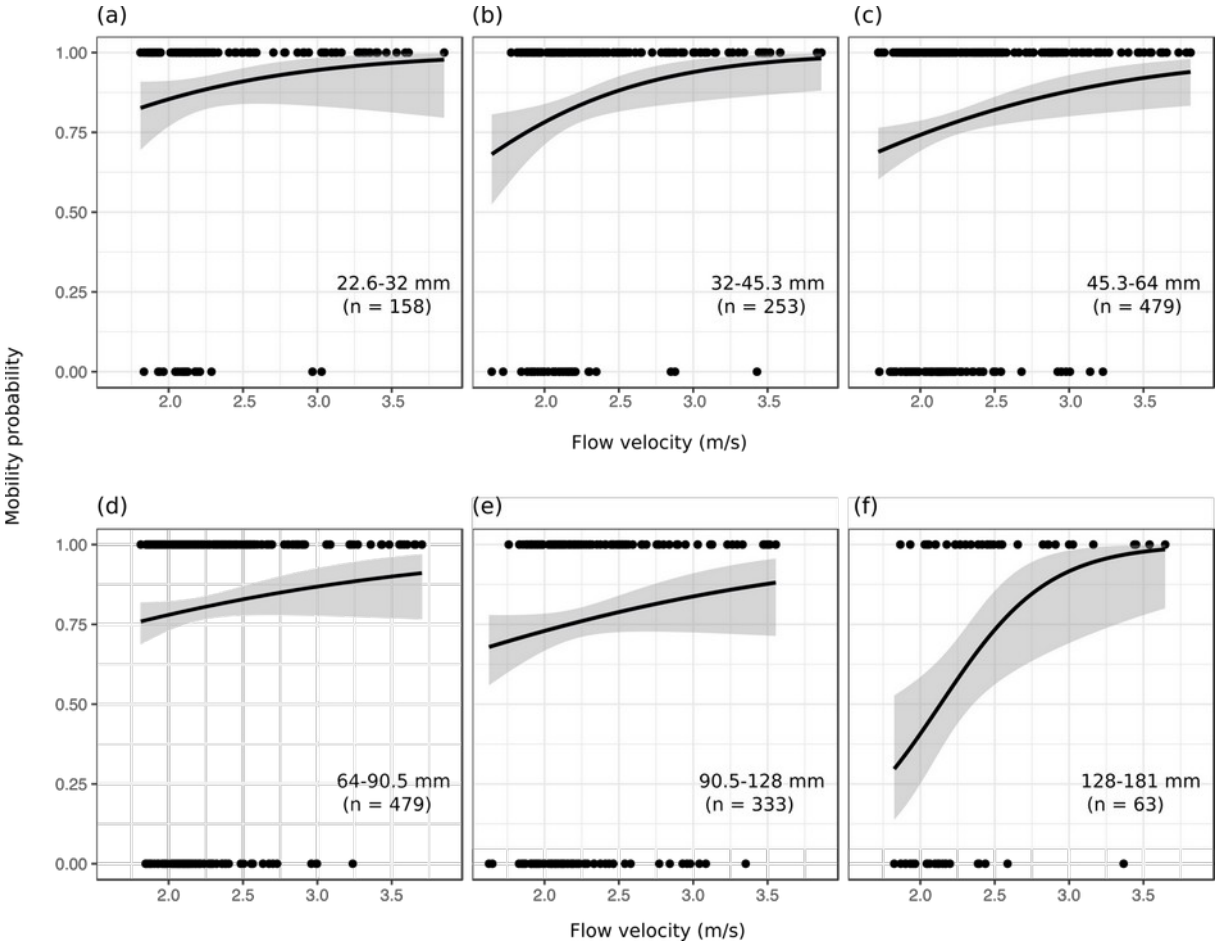

Figure 6: Logistic regressions of the tracer mobility according to flow velocity at their initial positions on the three SDs for peak floods during P_1 as a function of their grain size classes. Grey areas indicate the 95% confidence level of the logistic regression lines.

3.1.4 Assessment of suitable areas for implementing SDs according to flow velocity

In order to define the best areas in terms of hydraulic conditions for implementing future GAs on the Old Rhine, we used the empirical relationship found between the measured eroded areas and the maximum flow velocity. The critical flow velocity was fixed to 2.5 m.s^{-1} as shown in Section 4.1.3 (Figure 5.a and Figure 6). For a modeled discharge equal to the Q_2 flood, the mean value of the Suitability Index Ratio (SIR) calculated on elementary reach of

500 m length is equal to 0.59 with minimum and maximum values of 0.11 and 0.93, respectively (Figure 7). The majority of the upstream reaches of Kembs I2 were characterized by values lower than the mean SIR and inversely for the downstream reaches of Kembs I2. Moreover, our analysis showed that the velocity values were systematically lower than 2.5 $m.s^{-1}$ along the emerged bars at low flow for this modeled discharge.

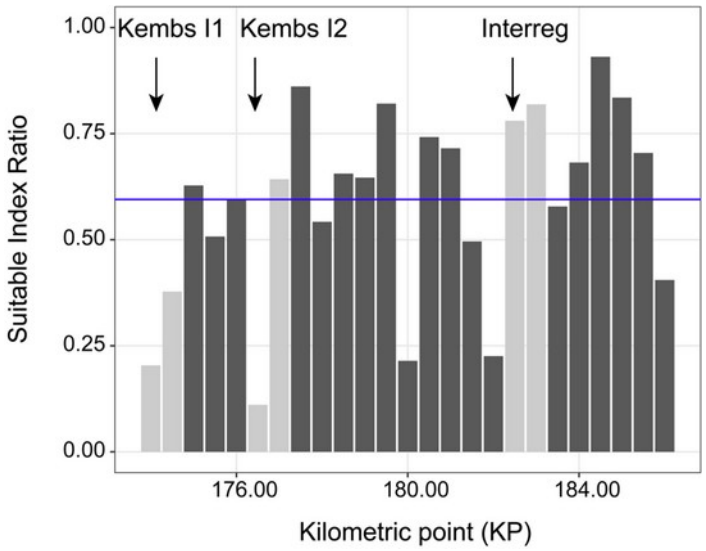

Figure 7: Longitudinal distribution of the SIR value for a Q_2 flood along the bypassed reach for each elementary reach of 500 m length. The blue line corresponds to the mean value of the SIR, black arrows locate the three SDs and gray bars are the reaches covered (completely or partly) by the SDs.

3.2 Monitoring of the downstream channel reaches

3.2.1 Assessment of tracer mobility

The tracer recovery rates ranged between 11% and 43% on the three studied reaches over the monitoring periods (Table 3). The recovery rates globally decreased over time, which was notably due to the decrease in the sampling pressure related to the tracer cloud propagation (Table 5). Translation occurred in the upstream part of the Interreg reach during P_1 and P_2 (Figure 8.a-b). During P_3 and P_4, tracers travelled through a clear translation-

dispersion mode (Figure 8.c-d). During P_5, the sediment pulse showed a fragmentation mode with preferential tracer deposition on riffles (Figure 8.e). For Kembs I1, a translation-dispersion mode also occurred during P_1, with only local translation in the medium part of the SD due to higher local flow velocities (Figure 8.f). During P_2, the distribution again showed a translation-dispersion pulse materialized by a heavy-tailed distribution due to a lower mobility of the tracers as some of them were trapped in the residual SD (Figure 8.i). The heavy-tailed distribution can be explained by (i) a lower mobility of tracers trapped in the residual SD in comparison with tracers traveling in the water channel (Liébault et al., 2012) or by (ii) a bedload partial mobility (Church & Hassan, 1992; Lenzi, 2004; Hassan et al., 2013; Schneider et al., 2014). For Kembs I2, the displacement of the tracer cloud showed a translation-dispersion pulse during P_1, with local translation in the upstream part of the SD due to higher velocities (Figure 8.h).

Gravel augmentation	Period	Qp ($m^3.s^{-1}$)	Qi ($m^3.s^{-1}$)	Number of days > Qc	Recovery rate (%)	Number of same tracers between two successive surveys	Travel distance of the tracer cloud centroid (m)	Maximum downstream tracer position (m)	Standard deviation of tracer cloud (m)
Kembs I1	P_{0bis}	-	-	-	-	-	-	394	128
Kembs I1	P_1	1630	~Q_3	25	42	625	194	791	165
Kembs I1	P_2	1842	~Q_4	55	42	368	390	4166	674
Kembs I2	P_{0bis}	-	-	-	-	-	-	450	143
Kembs I2	P_1	1842	~Q_4	54	33	501	138	2260	317
Interreg	P_{0bis}	-	-	-	-	-	-	604	189
Interreg	P_1	1080	<Q_2	5	43	644	101	682	129
Interreg	P_2	1340	<Q_2	20	12	111	232	1042	156
Interreg	P_3	1500	~Q_2	24	11	48	302	1982	370
Interreg	P_4	2480	~Q_{15}	29	15	39	1022	3677	611
Interreg	P_5	1842	~Q_4	106	18	58	1034	12099	2487

Table 5 : Statistical parameters for each sediment tracking survey conducted on each GA. The Interreg results between P_1 and P_4were provided by Arnaud et al. (2017).

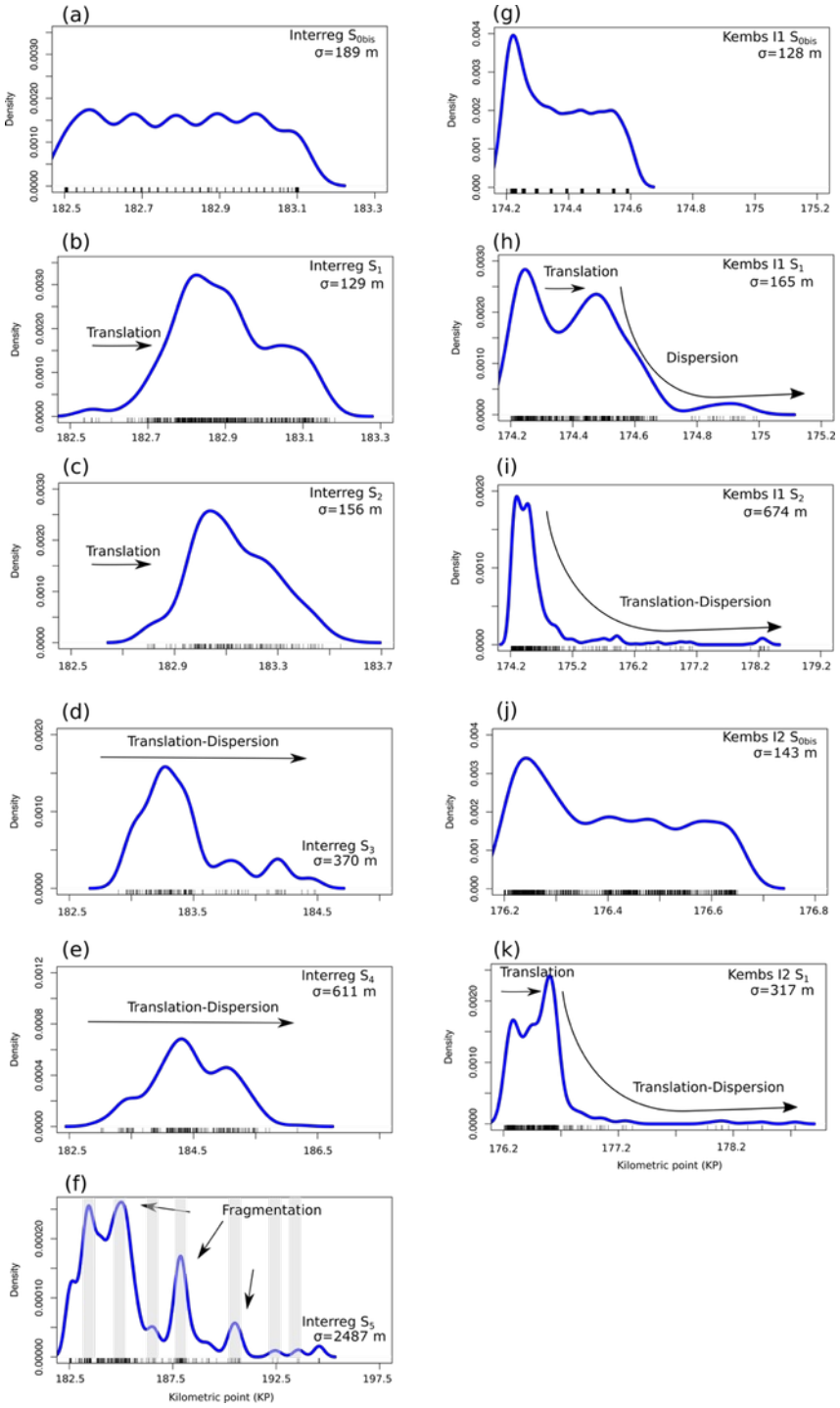

Figure 8: Probability density function of the longitudinal position of the tracers recovered for each survey on the (a-f) Interreg, where gray columns locate riffles, (g-i) Kembs I1 and (j-k) Kembs I2 downstream reaches.

The tracer cloud centroids travelled between 101 m and 390 m for moderate floods (Qix $\leq$ Q_4) on the three GA reaches. During the highest flood in May 2013, the tracer cloud centroid

of the Interreg reach travelled up to 1022 m. The farthest travelling tracer was found 12099 m downstream (Table 3). A statistically significant negative correlation (95% confidence level) following a power function was found between the virtual velocities and the cumulative excess stream energy on the Interreg reach (R^2 = 0.95, p-value=0.023) (Figure 9.a). We did not take into account P_4 because the peak flow was significantly higher than that for the other periods (~Q_{15}), inducing different bedload processes (Figure 9.a). The virtual velocity decreased over time (except for P4) with 2.34 m.h^{-1}, 0.96 m.h^{-1}, 0.95 m.h^{-1}, 2.44 m.h^{-1} and 0.57 m.h^{-1} for P_1, P_2, P_3, P_4 and P_5, respectively. Inter–GA comparison showed that the virtual velocities were lower for Kembs I1 and Kembs I2 than for Interreg for a similar range of cumulative excess stream energy with 0.54 m.h^{-1}, 0.38 m.h^{-1} and 0.13 m.h^{-1} for the P_1 of Kembs I1, the P_2 of Kembs I1 and the P_1 of Kembs I2, respectively. Comparison of our virtual velocity dataset with the literature suggests that our values are close to those of studies on riffle-pool rivers (Figure 9.b) (Gintz et al., 1996; Haschenburger and Church, 1998; Hassan et al., 1992; Houbrechts et al., 2015; Lamarre and Roy, 2008), except for Kembs I2, where the virtual velocity during P_1 is the lowest, comparable to steep-pool streams. In our case, the decrease in the virtual velocities was inversely correlated with the excess flood energy.

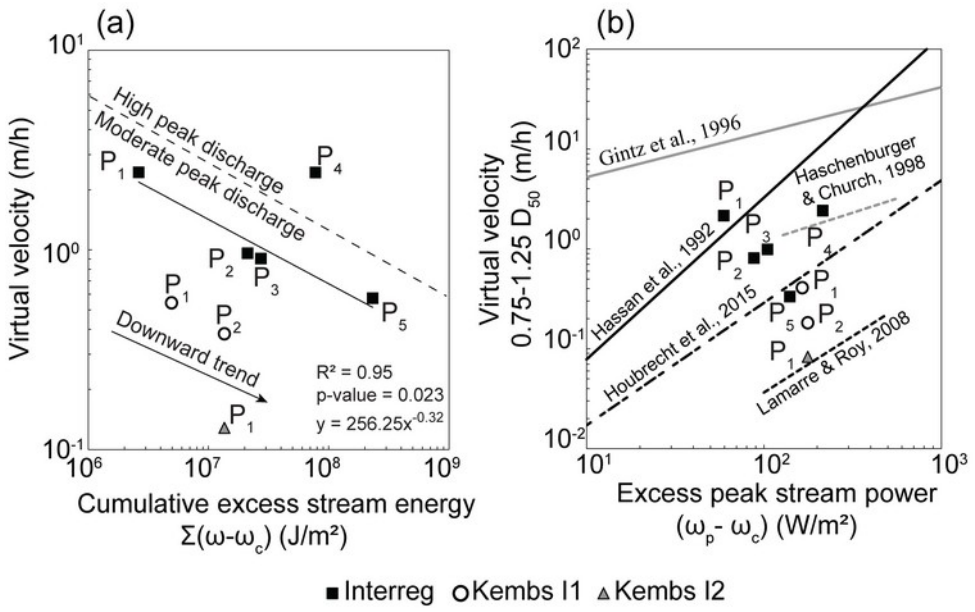

517

518 Figure 9: (a) Virtual velocity of the tracer cloud centroids for each *Pi* according to the
519 cumulative excess stream energy and (b) virtual velocity of the tracer cloud centroids
520 composed of tracers whose grain size ranges between 0.75 and 1.25 of the channel bed D_{50}
521 as a function of the excess unit stream power for each Pi (modified after Houbrechts et al.,
522 2015). The class 22.6-32 mm of Kembs I1 and Kembs I2 was excluded to make possible
523 comparisons with Interreg.

524 No relationship between the dimensionless travel distance of the tracer cloud centroid and
525 the grain size classes of recovered tracers was found for Kembs I1 during P_1, while a relation
526 was observed during P_2, indicating a partial mobility for this period (Figure 10). For Kembs
527 I2, a marked negative relationship is observed between the two variables during P_1, also
528 indicating selective sediment transport. For Interreg, no relationship was found between the
529 two variables up to P_4. Thereafter, a marked negative relationship was established during P_5
530 , again showing selective transport.

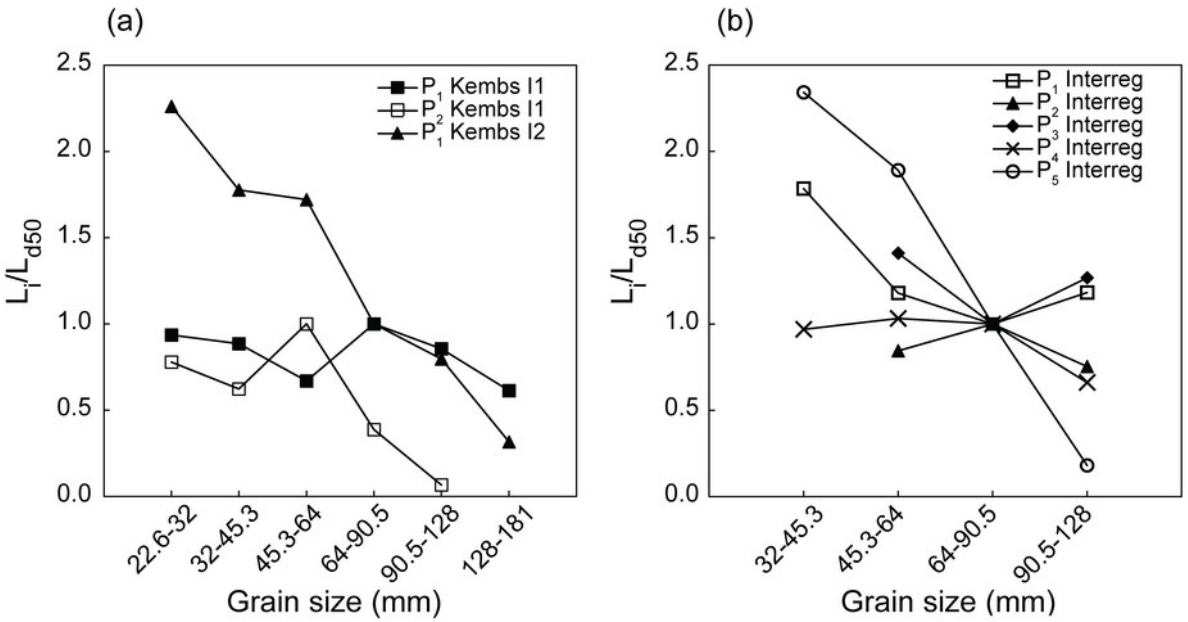

Figure 10: Mean dimensionless travel distance of the tracer cloud centroid for each grain size class, (a) for Kembs I1 and Kembs I2 and (b) for Interreg. Tracer clouds composed of less than 10 particles were excluded from the analysis because they were considered not statistically significant. For Kembs I1, only tracers recovered in the channel were included in the analysis.

3.2.2 Assessment of spatiotemporal grain size evolution

On a gravel bar sampled in the upstream part of the Interreg surveyed reach, the D_{95} decreased from S_0 to S_3 - S_4 (Figure 11.a). The grain size fining reached 36 mm between S_0 and S_3 and 53 mm between S_0 and S_4. New coarsening appeared in S5 with grain size values close to the S_0 values. For Kembs I2, a statistically significant bed fining (95% confidence interval) was observed (Kruskal-Wallis test, p-value < 0.0001) between S_0 and S_1, with a decrease in the mean D_{50} of the ten largest particle samples from 110 to 84 mm (Figure 11.b);. In S_0, a downstream grain size coarsening (from KP 176.3 to KP 177.5) was observed and was probably related to the downstream increase in the flow velocities (Figure 11.c). In S_1, a statistically significant downstream bed fining (95% confidence level) was observed (R^2 = 0.26; p-value < 0.016). The bed fining may be related to the partial mobility identified by the

bedload tracking surveys on the Kembs I1 surveyed reach during P_2, and the Kembs I2 surveyed reach during P_1 (see Section 3.2.1).

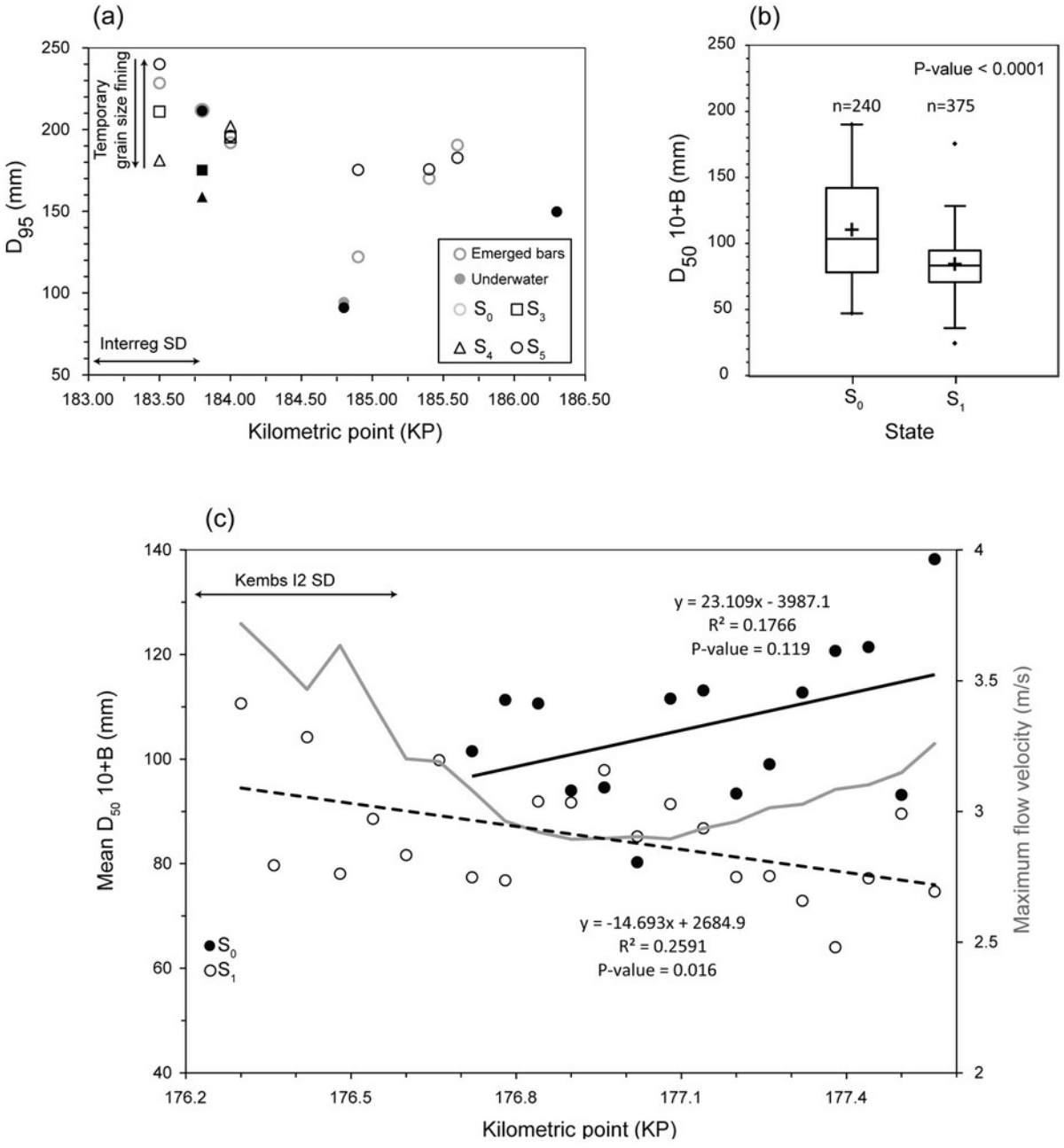

Figure 11: (a) D_{95} measured on each macroform and each survey along the Interreg restored reach with filled and empty symbols indicating the underwater and emerged samplings, respectively. (b) Boxplots of the D_{50} of the ten largest particles digitalized on each underwater digital image close to and downstream of the Kembs I2 SD for S_0 and S_1 and (c) D_{50} of the ten largest particles digitalized on each underwater digital image for S_0 and S_1

555 close to and downstream of the Kembs I2 SD; the gray line indicates the maximum velocity
556 for the peak flow during P_1 for each grain size transect; the black line and black dashed line
557 correspond to the linear regression lines of $S_0$and S_1, respectively.

558 3.2.3 Assessment of the spatiotemporal evolution of the channel diversity

559 Figure 12 shows the temporal and longitudinal evolution of the cumulative differences in the
560 cross-section diversity index (CSD) between 1985/93-2009 and the successive monitoring
561 surveys along the three restored reaches. The results show a negative downstream trend in
562 the cumulative differences of the post-GA index along all the reaches, which is an inverse
563 tendency by comparison with the 1985/93-2009 dataset. Moreover, the rates of changes
564 were higher after GA compared with those in the historical dataset. The results for the
565 Interreg reach show that the negative trend intensity decreased over time due to the
566 sediment dispersion along the channel bed. Marked positive trends of the index were first
567 observed in S_5 (Figure 12.a), which seems to be correlated to the fragmentation of the
568 bedload pulse (Figure 8.f).

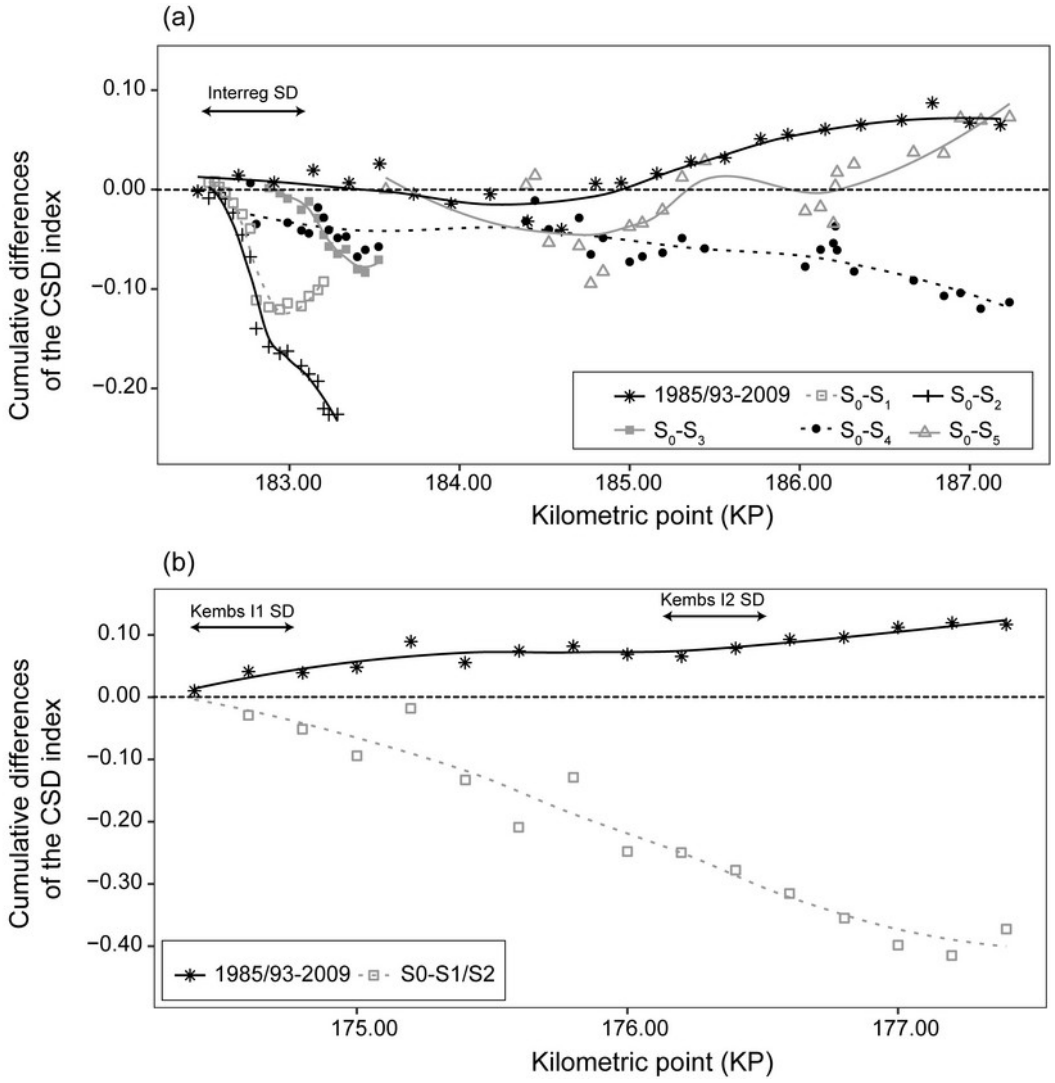

Figure 12: Cumulative differences in the CSD between the initial state and the successive surveys in the downstream direction (a) for the period 1985/93 - 2009 and S_0 to S_5 for the Interreg restored reach and (b) for the period 1985/93 – 2009 and S_0 to S_2 for Kembs I1 and S_0 to S_1 for Kembs I2.

4. Discussion

4.1 Optimal stockpile deposit design

The topo-bathymetric monitoring showed that the erosion of the three SDs included two processes closely interlocked: SD toe erosion and mass failure. This is consistent with

previous field and modeling studies on GA operations (Battisacco, 2016; Heckmann et al., 2017). Battisacco et al, (2016) and Vonwiller et al, (2018) showed that toe erosion is the predominant process, followed by the mass failure of the upper part of the SD. In our case, both processes occurred from a flow velocity of 2.5 $m.s^{-1}$ (Figure 5.a), which caused full mobility of the introduced sediment (Figure 6). For flow velocities lower than this critical value, only a limited toe erosion was observed with a selective mobility of gravels, which generated a reduction in the erosion intensity and the establishment of a coarser layer on the residual SD, as observed in the upstream and downstream part of Kembs I1 (Figure 3.b). This coarser layer can significantly reduce the erosion of the residual SD during future flood events, as observed in studies conducted on sediment starved rivers (Rollet et al. 2013; Houbrechts et al. 2012), and explain the lower eroded volumes during P_2 compared to P_1, despite higher and longer flood events (Figure 2.a).

These results highlight the fact that SDs should be implemented/designed in suitable hydraulic areas to maximize the SD erosion probability for a $Q_{1\text{-}2}$ flood, considering that entrainment must be performed for frequent floods to avoid any risk of vegetation encroachment and increase in phytostabilization. Based on the critical flow velocities (Figure 5 and Figure 6), we determined the suitable areas for GA along the first 15 km of the studied reach (Figure 7). From this study, we estimate that the potentially suitable areas correspond to 53% of the study area. This approach is useful to plan further GAs in the Old Rhine, and it should be transferable to other rivers. Our results also show that SD implementation on bars is not suitable for a Q_2 peak flow due to flow velocities lower than the critical value.

599 **4.2 Bedload transport patterns**

600 At a short term (1 to 3 years), our results show that the mode of sediment transfer varies
601 among a translation pulse for Interreg and a combination of translation and dispersion for
602 Kembs I1 and Kembs I2 (Figure 8). Such processes were also observed in both modeling (Koll
603 et al., 2010; Sklar et al., 2009) and field studies on GA operations (Downs et al., 2016). The
604 mode of sediment pulse depends on the grain size of the introduced sediment compared to
605 the predisturbance in-channel grain size, sediment sorting and sediment volume (Lisle et al.,
606 2001; Sklar et al., 2009; Sims et al., 2017). Dispersion occurs in high bed roughness contexts
607 and when the input volumes exceed the bedload transport capacity (Lisle et al., 2001; Sims
608 et al., 2017). At mid-term (~ 5 years), the mode of sediment pulse for the Interreg GA was
609 non-random and fragmented (Gaeuman et al., 2017), driven by the bed morphology,
610 particularly riffle-pool sequences (Sear, 1996) (Figure 8).
611 Virtual velocities show the same order of magnitude as those in other studies conducted on
612 riffle-pool rivers for the same exceeding peak flow energy, which indicates that the GA
613 sediment transport dynamics were equivalent to the sediment mobility in natural conditions.
614 A decrease in the virtual velocities occurred during the monitoring period despite the
615 increase in the excess flow energy (Figure 9.a). This decreasing tendency of sediment
616 mobility over time was observed in other field studies (Ferguson et al., 2002; Haschenburger,
617 2011) and modeling works (Koll et al., 2010). This tendency is explained by a vertical mixing
618 of gravels where tracers are progressively buried, which reduces their mobility (Ferguson et
619 al. 2002). Sediment mobility can also be slowed by the bed roughness (Hassan et al., 1991)
620 and the variability in the bed morphology (Pyrce and Ashmore, 2003; Sear, 1996). The
621 relations between bedload mobility and hydrology are more complex because of numerous
622 determinant parameters, such as peak flow intensity, hydrogram shape (duration and peak

number) and initial conditions, such as low flow duration preceding the flood event and sediment transport processes during the previous morphogenic flood (Humphries et al., 2012). Vázquez-Tarrío et al. (2018) showed on the Rhône River that a coarser armor layer is frequently located just below dams due to the propagation of sediment starvation conditions in the downstream direction. Rollet et al. (2013) observed on the Ain River that sediment tracers travel relatively slowly on sediment-starved reaches due to sediment trapping in the interstices of the armor layer. Thus, the differences in the sediment pulse patterns and the virtual velocities among the three GAs can be explained by both lower bedload transport capacities and higher bed roughness for Kembs I1 and I2 compared to Interreg. Overall, the results reinforce the conclusions of Arnaud et al. (2017) that no important sediment volumes travel rapidly downstream in the Old Rhine. Consequently, there is no risk of navigation perturbations downstream of the Breisach dam (Figure 1).

4.3 Channel morphodynamic responses

In the short term, a significant bed grain size fining was observed in the channel and on some emerged bars (Figure 11.a-b-c), while the topo-bathymetric results revealed a simplification of the channel bed geometry (Figure 12). These results are consistent with a modeling study conducted by Battisacco et al. (2016), which demonstrated that SDs having characteristics similar to ours produce sediment spreading along the restored reach, thus favoring bed grain size fining and a limitation in the bed incision tendency rather than increasing habitat heterogeneity. At mid-term, the grain size fining observed in the Interreg reach was temporary due to the downstream bedload transfer without any new supply. A relationship appeared between the dimensionless distances of the tracers and their grain size when the dispersion was advanced (Figure 10), indicating a partial mobility (Church and

Hassan, 1992). This may reveal the formation of a new armor layer due to new sediment starvation conditions explained by the lack of upstream sediment supply (Piégay et al., 2016). All results show that the positive geomorphic effects of the three GAs are transitory, with a duration of approximately 3-4 flood events depending on the remobilized sediment volumes, the flow velocities and the bedload transport processes (Sklar et al., 2009). An increase in the channel diversity downstream of the Interreg SD occurred due to a preferential sediment deposition on riffles (Figure 12) and explain notably by lower flow velocities and shear stresses than in pools during flood events (Sear, 1996). This result indicates that a diversified downstream channel morphology tends to enhance the positive morphological effects of GAs and should be taken into account, in addition to local flow conditions around the SDs, for designing GA operations.

The sediment wave fragmentation along the Interreg reach has been highlighted because the monitoring was conducted over a long period (7 years) and an important channel length (maximum of 12 km). Thus, monitoring must be performed on extended lengths (several kilometers) and over mid to long temporal scales to adequately evaluate the effects of GAs. We can hypothesize that a fragmentation of the sediment wave of both of the Kembs GAs will also occur more or less rapidly depending on flow conditions.

Our results showed that even if GA operations are repeated over time in the Old Rhine, it is unlikely that a sustainable diversification of aquatic habitats may be obtained due to the narrow and homogeneous channel geometry of the study reach. Channel widening by removal of bank protection, partial removal of groin fields and/or excavation of floodplain areas connected to the channel should be tested downstream of GAs so as to promote a reduction and a diversification of flow conditions, inducing the deposition of a part of the introduced sediments and potentially creating new fluvial forms, such as side channels and

bars colonizable by pioneer vegetation (Arnaud et al., 2017; Staentzel et al., 2018b). Sediment excavated from channel widening should be stored temporarily and introduced upstream with a rhythm depending on the hydrological regime. The success of this mode of sediment management has been demonstrated along the Mur River by Klösch (2011), which highlighted that channel widening locally decreased the bedload transport capacity of the river, favoring bedload deposition and, consequently, local bank erosion as a positive retroaction loop. However, the self-sustaining of geomorphic processes is strongly dependent on the upstream bedload supply (Klösch, 2011).

In terms of risks, our results show that the evolution of channel topography at the mid-term is relatively low (Figure 12). Our results confirm the absence of risk of uncontrolled bed degradation, which was also noticed by Arnaud et al. (2017) over a shorter monitoring period for the Interreg GA. Furthermore, the hydrological functioning of the excavated areas in terms of flow retention may not be impacted either. In addition, no significant bank erosion was observed during the monitoring period.

4.4 Recommendations and management scenario to improve the efficiency and sustainability of GAs

Following this study, several recommendations and management scenario can be addressed for improving the efficiency of GA operations and the sustainability of their effects at the scale of the SDs as well as the scale of the downstream reach:

1. perform hydraulic modeling to identify the most suitable areas for SD implementation;

2. on this basis, prioritize areas with high flow velocities during frequent floods to implement SDs to limit the risk of SD fixation accentuated by the development of the vegetation;
3. adapt the grain size of the GAs to the local flow competence to minimize the risk of the formation of a coarser layer at the top of the residual SD, which would decrease the SD erodibility;
4. implement SDs upstream of reaches showing the highest diversity of macroforms and flow conditions to favor a fragmentation of the sediment transport and thus maximize potential habitat diversification, notably by bed grain size fining.
5. Test channel widening downstream of GAs to lower flow conditions, and to induce sediment deposition (and a general slowdown of the sediment waves), the establishment of pioneer vegetation and the diversification of aquatic and riverine habitats (Arnaud et al. 2017), as bars and secondary channels (Figure 13.a). Sediment deposition may also induce local bar/bank erosion, provoking local bedload supply into the channel in a positive feedback loop. Widening areas should be performed ideally close to riffles to reinforce the sediment wave fragmentation by gravel deposition, extending spawning areas for salmonid fish species. Riffle aggradation and bar formation may also foster hyporheic water exfiltration areas, which are summer thermal refuges favoring the adaptation of aquatic ecosystems to climate change (Eschbach et al., 2017). Furthermore, habitat diversification may also limit the relative development of invasive species (Staentzel et al., 2018a) and raise the recreative value of the Old Rhine (Arnaud et al., 2017). The resulting excavated sediments should be stored temporarily close to the channel and introduced upstream iteratively (Figure 13.a.2). This management scenario would increase both

the extent and the durability of the GA benefits, in comparison with the management scenario consisting only in GA (Figure 13.b).

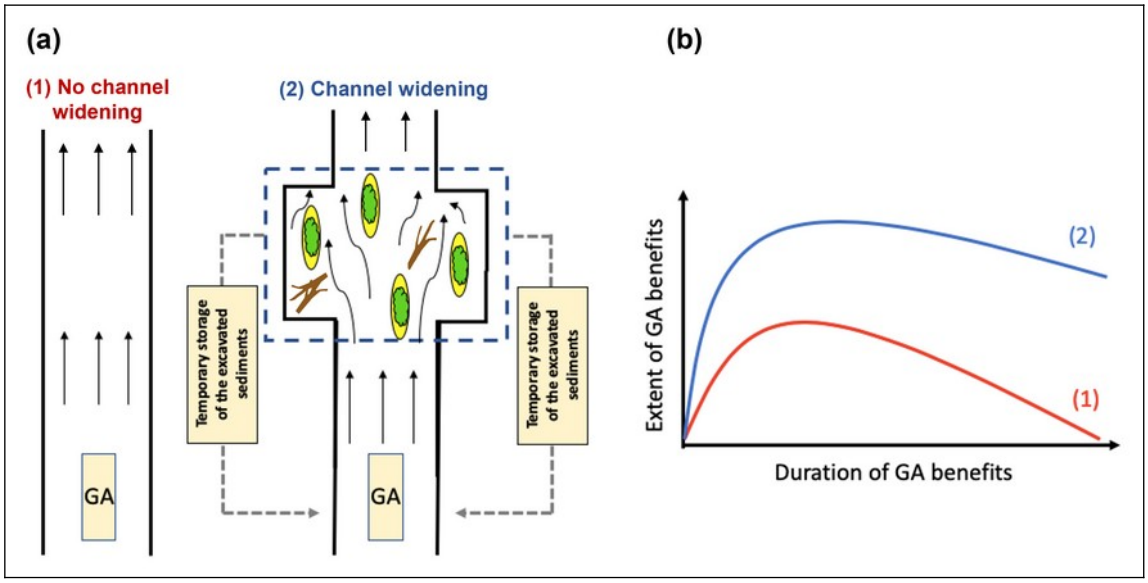

Figure 13: (a) Restoration scenarios based on 1-GA only, 2-combination of GA with downstream channel widening, (b) benefits of both scenarios in terms of spatial extent and duration.

5. Conclusions

This study provides original feedback based on multi-compartment monitoring of three *in situ* GAs conducted along the bypassed section of the Rhine River downstream of Kembs, notably in terms of SD erodibility, sediment transport dynamics and channel responses. The erosion of SDs is dependent on local flow velocities and also on the grain size of the introduced sediment according to the local transport capacity. The Interreg GA was the best GA design compared to the two others. More generally, 53% of the 15 km upstream of the Old Rhine are suitable to implement GAs for flood flows or higher Q_2. Along the reaches affected by the GAs in the short term, bathymetric simplification was observed due to the transfer of sediments mostly along the thalweg and a transitory grain size fining. At mid-

term (~ 5 years), local habitat diversification was observed due to fragmentation of the sediment wave with preferential bedload deposition on riffles, which is a positive effect for fish spawning habitats. Our results also show that GAs induce no risk for human activities. This study highlights that to improve restoration efficiency and sustainability, GAs must be implemented in upstream reaches characterized by the highest hydromorphological diversity to increase positive effects. However, new sediment starvation conditions appeared > 5 years due to the lack of upstream sediment supply, showing that GAs must be repeated over time. To increase the efficiency of GA operations, channel widening should be performed downstream of the GAs to improve the sustainability of the GA effects. Sediment excavated from channel widenings should be stored temporarily and introduced upstream iteratively.

References

Arnaud F. 2012. Historical and Experimental Geomorphology for the Process-based Restoration of a Modified Fluvial System: the Old Rhine Between Kembs and Breisach (France, Germany), PhD Dissertation. University of Lyon (in French with English abstract).

Arnaud, F., Piégay, H., Béal, D., Collery, P., Vaudor, L., Rollet, A.-J., 2017. Monitoring gravel augmentation in a large regulated river and implications for process-based restoration: Monitoring gravel augmentation in a large regulated river. Earth Surf. Process. Landforms 42, 2147–2166. https://doi.org/10.1002/esp.4161

Arnaud, F., Piégay, H., Schmitt, L., Rollet, A.J., Ferrier, V., Béal, D., 2015a. Historical geomorphic analysis (1932 – 2011) of a by-passed river reach in process-based restoration perspectives : The Old Rhine downstream of the Kembs diversion dam (France , Germany). Geomorphology 236, 163–177.

https://doi.org/10.1016/j.geomorph.2015.02.009

Arnaud, F., Piégay, H., Vaudor, L., Bultingaire, L., Fantino, G., 2015b. Technical specifications of low-frequency radio identification bedload tracking from field experiments: Differences in antennas, tags and operators. Geomorphology 238, 37–46. https://doi.org/10.1016/j.geomorph.2015.02.029

Arnaud, F., Schmitt, L., Johnstone, K., Rollet, A., Piégay, H., 2019. Geomorphology Engineering impacts on the Upper Rhine channel and floodplain over two centuries. Geomorphology 330, 13–27. https://doi.org/10.1016/j.geomorph.2019.01.004

Battisacco, E., Franca, M.J., Schleiss, A.J., 2016. Sediment replenishment: Influence of the geometrical configuration on the morphological evolution of channel-bed. Water Resour. Res. 52. https://doi.org/10.1002/2016WR019157

Bennett, G.L., Molnar, P., Eisenbeiss, H., Mcardell, B.W., 2012. Erosional power in the Swiss Alps: Characterization of slope failure in the Illgraben. Earth Surf. Process. Landforms 37, 1627–1640. https://doi.org/10.1002/esp.3263

Béraud C. 2012. Numerical Modelling of Sediment Feeding Impacts in Engineered Rivers. The Case of the Old Rhine Between Kembs and Breisach, PhD Dissertation. University of Lyon (in French with English abstract).

Brasington, J., Langham, J., Rumsby, B., 2003. Methodological sensitivity of morphometric estimates of coarse fluvial sediment transport. Geomorphology 53, 299–316. https://doi.org/10.1016/S0169-555X(02)00320-3

Brousse, G., Arnaud-Fassetta, G., Liébault, F., Bertrand, M., Melun, G., Loire, R., Malavoi, J.R., Fantino, G., Borgniet, L., 2019. Channel response to sediment replenishment in a large

777 gravel-bed river: The case of the Saint-Sauveur dam in the Buëch River (Southern Alps,
778 France), in: River Research and Applications. 1-14. https://doi.org/10.1002/rra.3527

779 Chardon, V., Schmitt, L., Piégay, H., Lague, D., 2020. Use of terrestrial photosieving and
780 airborne topographic LiDAR to assess bed grain size in large rivers: a study on the Rhine
781 River. Earth Surf. Process. Landforms. https://doi.org/10.1002/esp.4882

782 CHR. 2009. Erosion, Transport and Deposition of Sediment – Case Study Rhine, Report II-20.
783 CHR/KHR: Lelystad.
784 Church, M., Mclean, D., Wolcott J.F, 1987. River Bed Gravels: Sampling and Analysis.
785 Church, M., Hassan, M.A., 1992. Size and Distrance of Travel Unsconstrained Clasts on a
786 Streambed. Water Resour. Res. 28, 299–303. https://doi.org/10.1029/91WR02523
787 Cooper, A.R., Infante, D.M., Daniel, W.M., Wehrly, K.E., Wang, L., Brenden, T.O., 2017.
788 Assessment of dam effects on streams and fish assemblages of the conterminous USA.
789 Sci. Total Environ. 586, 879–889. https://doi.org/10.1016/j.scitotenv.2017.02.067
790 Douglas L. Inman, 1952. Measures for Describing the Size Distribution of Sediments. SEPM J.
791 Sediment. Res. Vol. 22, 125–145. https://doi.org/10.1306/D42694DB-2B26-11D7-
792 8648000102C1865D
793 Downs, P.W., Keele, V.E., Gilvear, D.J., 2016. Dispersal of augmented gravel in a steep ,
794 boulder-bedded reach : early implications for restoring salmonid habitat. Proceedings
795 11th International Symposium on Ecohydraulics (ISE 2016).
796 Dittrich A., Koll K., Kunz C., 2010. Historische Entwicklung des südlichen Oberrheins unter
797 morphologischen Gesichtspunkten. Bericht Nr. 985. Leichtweiss-Institut für Wasserbau,
798 Technische Universität Braunschweig, 38 p
799 El kadi Abderrezzak K. 2009. Estimate of Bedload Transport Capacity in the Old Rhine

Between Kembs and Breisach, Report H-P73–2009- 00402-FR. EDF R&D: Chatou (in French with English abstract).

Eschbach, D., Piasny, G., Schmitt, L., Pfister, L., Grussenmeyer, P., Koehl, M., Skupinski, G., Serradj, A., 2017. Thermal-infrared remote sensing of surface water–groundwater exchanges in a restored anastomosing channel (Upper Rhine River, France). Hydrol. Process. 31, 1113–1124. https://doi.org/10.1002/hyp.11100

Ferguson, R.I., Bloomer, D.J., Hoey, T.B., Werritty, A., 2002. Mobility of river tracer pebbles over different timescales. Water Resour. Res. 38, 3–8. https://doi.org/10.1029/2001wr000254

Foley, M.M., Magilligan, F.J., Torgersen, C.E., Major, J.J., Anderson, C.W., Connolly, P.J., Wieferich, D., Shafroth, P.B., Evans, J.E., Infante, D., Craig, L.S., 2017. Dam removal-listening in Landscape context and the biophysical response of rivers to dam removal in the United States.PLOS ONE. https://doi.org/10.1371/journal.pone.0180107

Gaeuman D. 2013. Monitoring the Effectiveness of Gravel Augmentations for Salmonid Habitat Improvement Downstream from Dams, Completion Report Project 0295. US Bureau of Reclamation Science and Technology: Washington, DC.

Gaeuman D. 2014. High-flow gravel injection for constructing designed in-channel features. River Research and Applications 30, 685–706. https://doi.org/10.1002/rra.2662

Gaeuman, D., Stewart, R., Schmandt, B., Pryor, C., 2017. Geomorphic response to gravel augmentation and high - flow dam release in the Trinity River , California 2540, 2523–2540. https://doi.org/10.1002/esp.4191

Garnier, A., Barillier, A., 2015. The Kembs project: environmental integration of a large existing hydropower scheme. La Houille Blanche 21–28. https://doi.org/10.1051/lhb/20150041

824 Gintz, D., Hassan, M.A., Schmidt, K.H., 1996. Frequency and magnitude of bedload transport
825 in a mountain river. Earth Surf. Process. Landforms 21, 433–445.
826 https://doi.org/10.1002/(SICI)1096-9837(199605)21:5<433::AID-ESP580>3.0.CO;2-P
827 Gostner, W., Alp, M., Schleiss, A.J., Robinson, C.T., 2013. The hydro-morphological index of
828 diversity: a tool for describing habitat heterogeneity in river engineering projects.
829 Hydrobiologia 712, 43–60. https://doi.org/10.1007/s10750-012-1288-5
830 Haschenburger, J.K., 2011. The rate of fluvial gravel dispersion. Geophys. Res. Lett. 38
831 https://doi.org/10.1029/2011GL049928
832 Haschenburger, J.K., Church, M., 1998. Bed material transport estimated from the virtual
833 velocity of sediment. Earth Surf. Process. Landforms. 23, 791-808.
834 https://doi.org/10.1002/(SICI)1096-9837(199809)23:9<791::AID-ESP888>3.0.CO;2-X
835 Hassan, M.A., Church, M., Ashworth, P.J., 1992. Virtual rate and mean distance of travel of
836 individual clasts in gravel-bed channels. Earth Surf. Process. Landforms 17, 617–627.
837 https://ui.adsabs.harvard.edu/link_gateway/1992ESPL...17..617H/doi:10.1002/
838 esp.3290170607
839 Hassan, M.A., Church, M., Schick, A.P., 1991. Distance of movement of coarse particles in
840 gravel bed streams 27, 503-511. https://doi.org/10.1029/90WR02762

841 Hassan, M.A., Voepel, H., Schumer, R., Parker, G., Fraccarollo, L., 2013. Displacement
842 characteristics of coarse fluvial bed sediment. JOURNAL OF GEOPHYSICAL
843 RESEARCH: EARTH SURFACE, Vol.118, 155–165.
844 https://doi.org/10.1029/2012JF002374

845 Heckmann, T., Haas, F., Abel, J., Rimböck, A., Becht, M., 2017. Geomorphology Feeding the
846 hungry river : Fluvial morphodynamics and the entrainment of arti fi cially inserted

847 sediment at the dammed river Isar , Eastern 291, 128–142.
848 https://doi.org/10.1016/j.geomorph.2017.01.025
849 Houbrechts, G., Levecq, Y., Vanderheyden, V., Petit, F., 2011. Long-term bedload mobility in
850 gravel-bed rivers using iron slag as a tracer. Geomorphology 126, 233-244.
851 https://doi.org/10.1016/j.geomorph.2010.11.006
852 Houbrechts, G., Levecq, Y., Peeters, A., Hallot, E., Campenhout, J. Van, Denis, A., Petit, F.,
853 2015. Geomorphology Evaluation of long-term bedload virtual velocity in gravel-bed
854 rivers. Geomorphology 251, 6-19. https://doi.org/10.1016/j.geomorph.2015.05.012
855 Houbrechts, G., Van Campenhout, J., Levecq, Y., Hallot, E., Peeters, A., Petit, F., 2012.
856 Comparison of methods for quantifying active layer dynamics and bedload discharge in
857 armoured gravel-bed rivers. Earth Surf. Process. Landforms 37, 1501–1517.
858 https://doi.org/10.1002/esp.3258
859 Humphries, R., Venditti, J.G., Sklar, L.S., Wooster, J.K., 2012. Experimental evidence for the
860 effect of hydrographs on sediment pulse dynamics in gravel-bedded rivers. Water
861 Resour. Res. 48 https://doi.org/10.1029/2011WR010419
862 Juez, C., Battisacco, E., Schleiss, A.J., Franca, M.J., 2016. Advances in Water Resources
863 Assessment of the performance of numerical modeling in reproducing a replenishment
864 of sediments in a water-worked channel. Adv. Water Resour. 92, 10–22.
865 https://doi.org/10.1016/j.advwatres.2016.03.010
866 Klösch, M., Hornich, R., Baumann, N., Puchner, G., Habersack, H., 2011. Mitigating channel
867 incision via sediment input and self-initiated riverbank erosion at the Mur River, Austria.
868 Geophys. Monogr. Ser. https://doi.org/10.1029/2010GM000977
869 Koll K, Koll K, Dittrich A. 2010. Sediment transport over static armour layers and its impact on
870 bed stability. In Proceedings, 5th International Conference on Fluvial Hydraulics (River

Flow 2010), Dittrich A, Koll K, Aberle J, Geisenhainer P (eds). Bundesanstalt für Wasserbau: Braunschweig; 929–936.

Mathias Kondolf, G., Graham, W. V, Matthews, G., 1991. UC Berkeley.

Kondolf, G.M., 1997. Hungry water: Effects of dams and gravel mining on river channels. Environ. Manage. 21, 533-551 https://doi.org/10.1007/s002679900048

Kondolf, G.M., Gao, Y., Annandale, G.W., Morris, G.L., Jiang, E., Zhang, J., Cao, Y., Carling, P., Fu, K., Guo, Q., Hotchkiss, R., Peteuil, C., Sumi, T., Wang, H.-W., Wang, Z., Wei, Z., Wu, B., Wu, C., Yang, C.T., 2014. Sustainable sediment management in reservoirs and regulated rivers: Experiences from five continents. Earth's Futur. 2, 256–280. https://doi.org/10.1002/2013EF000184

Lamarre, H., Roy, A.G., 2008. The role of morphology on the displacement of particles in a step–pool river system. Geomorphology 99, 270–279. https://doi.org/10.1016/j.geomorph.2007.11.005

Landon, N., 2008. Du constat d'enfoncement du lit fluvial aux actions de recharge sédimentaire: quellessolutions pour une gestion raisonnée de nos cours d'eau? Outils de gestion de l'eau en territoire demontagne, PNR du Queyras, ONEMA et MEDR, pp.28-39, 2007. halshs-00279895

Lane, S.N., Westaway, R.M., Hicks, D.M., 2003. Estimation of erosion and deposition volumes in a large, gravel-bed, braided river using synoptic remote sensing. Earth Surf. Process. Landforms 28, 249–271. https://doi.org/10.1002/esp.483

Lenzi, M.A., 2004. Displacement and transport of marked pebbles , cobbles and boulders during floods in a steep mountain stream, Hydrol. Process. 18, 1899–1914 (2004). https://doi.org/10.1002/hyp.1456

Liébault, F., Bellot, H., Chapuis, M., Klotz, S., Deschâtres, M., 2012. Bedload tracing in a high-sediment-load mountain stream. Earth Surf. Process. Landforms 37, 385–399. https://doi.org/10.1002/esp.2245

Magilligan, F.J., Nislow, K.H., 2005. Changes in hydrologic regime by dams. Geomorphology 71, 61-78. https://doi.org/10.1016/j.geomorph.2004.08.017

Ock, G., Gaeuman, D., McSloy, J., Kondolf, G.M., 2015. Ecological functions of restored gravel bars, the Trinity River, California. Ecol. Eng. 83, 49–60. https://doi.org/10.1016/j.ecoleng.2015.06.005

Ock, G., Sumi, T., Takemon, Y., 2013. Sediment replenishment to downstream reaches below dams: implementation perspectives. Hydrol. Res. Lett. 7, 54–59. https://doi.org/10.3178/hrl.7.54

Pasternack, G.B., Wang, C.L., Merz, J.E., 2004. Application of a 2D hydrodynamic model to design of reach-scale spawning gravel replenishment on the Mokelumne River, California. River Res. Appl. 20, 205–225. https://doi.org/10.1002/rra.748

Petts, G.E., Gurnell, A.M., 2005. Dams and geomorphology: Research progress and future directions. Geomorphology 71, 27–47. https://doi.org/10.1016/j.geomorph.2004.02.015

Piégay, H., Aelbrecht, D., Béal, D., Alonso, C., Armburster, J., Arnaud, F., Béraud, C., Billard, C., Bouchard, J.P., Piégay, H., Aelbrecht, D., Béal, D., Alonso, C., Armburster, J., 2011. Restauration morpho-dynamique et redynamisation de la section court-circuitée du Rhin en aval du barrage de Kembs (projet INTERREG / EDF).

Piégay, H., Arnaud, F., Cassel, M., Depret, T., Alber, A., Michel, K., Rollet, A.-J., Vaudor, L., 2016. Suivi par RFID de la mobilité des galets: retour sur 10 ans d'expérience en grandes

rivières. BSGLg 67.

Pyrce, R.S., Ashmore, P.E., 2003. The relation between particle path length distributions and channel morphology in gravel-bed streams : a synthesis. Geomorphology 56, 167–187. https://doi.org/10.1016/S0169-555X(03)00077-1

Rempel, L.L., Church, M., 2009. Physical and ecological response to disturbance by gravel mining in a large alluvial river. Can. J. Fish. Aquat. Sci. 66, 52–71. https://doi.org/10.1139/F08-184

Rollet, A.j., 2007. Study and management of the sedimentary dynamics of a river section downstream of a dam: the case of the lower Ain Valley. PhD Dissertation. University of Lyon (in French with English abstract).

Rollet, A.J., Dufour, S., Bornette, G., Persat, H., 2013. Assessment of consequences of sediment deficit on a gravel river bed downstream of dams in restoration perspectives : application of a multicriteria , hierarchical and spatially explicit diagnosis. River Res. Appl 30, 939-953. https://doi.org/10.1002/rra

Schälchli, U., Breitenstein, M., Kirchhofer, A., 2010. Kiesschüttungen zur Reaktivierung des Geschiebehaushalts der Aare-die kieslaichenden Fische freut's. Wasser Energ. Luft 102, 209–213.

Schmitt, L., Morris, D., Kondolf, G.M., 2018. Managing floods in large river basins in Europe: The Rhine river, in: Managing Flood Risk: Innovative Approaches from Big Floodplain Rivers and Urban Streams. https://doi.org/10.1007/978-3-319-71673-2_4

Schneider, J.M., Turowski, J.M., Rickenmann, D., Hegglin, R., Arrigo, S., Mao, L., Kirchner, J.W., 1Mountain, 2014. Journal of Geophysical Research : Earth Surface. J. Geophys. Res. Earth Surf. 119, 2315–2334. https://doi.org/10.1002/2014JF003147.Received

Sear, D.A., 1996. Sediment transport processes in pool-riffle sequences. Earth Surf. Process.

Landforms 21, 241-262. https://doi.org/10.1002/(SICI)1096-9837(199603)21:3<241::AID-ESP623>3.0.CO;2-1

Sims, A., Sims, A.J., Rutherfurd, I.D., 2017. Management responses to pulses of bedload sediment in rivers Geomorphology Management responses to pulses of bedload sediment in rivers. Geomorphology 294, 70–86. https://doi.org/10.1016/j.geomorph.2017.04.010

Sklar, L.S., Fadde, J., Venditti, J.G., Nelson, P., Wydzga, M.A., Cui, Y., Dietrich, W.E., 2009. Translation and dispersion of sediment pulses in flume experiments simulating gravel augmentation below dams 45, 1–14. https://doi.org/10.1029/2008WR007346

Staentzel, C., Arnaud, F., Combroux, I., Schmitt, L., Trémolières, M., Grac, C., Piégay, H., Barillier, A., Chardon, V., Beisel, J.-N., 2018a. How do instream flow increase and gravel augmentation impact biological communities in large rivers: A case study on the Upper Rhine River. River Res. Appl. 34, 153-164 https://doi.org/10.1002/rra.3237

Staentzel, Cybill, Combroux, I., Barillier, A., Schmitt, L., Chardon, V., Garnier, A., Beisel, J.N., 2018b. Réponses des communautés biologiques à des actions de restauration de grands fleuves, La Houille Blanche 1–9. https://doi.org/10.1051/lhb/2018024

Stähly, S., Franca, M.J., Robinson, C.T., Schleiss, A.J., 2019. Sediment replenishment combined with an artificial flood improves river habitats downstream of a dam. Sci. Report 9, 5176. https://doi.org/10.1038/s41598-019-41575-6

Sumi, Tetsuya Masahisa Okano, Y.T., 2004. Proceedings of the Ninth International Symposium on River Sedimentation October 18 – 21, 2004, Yichang, China 1036–1043.

Vázquez-Tarrío, D., Tal, M., Camenen, B., Piégay, H., 2018. Effects of continuous embankments and successive run-of-the-river dams on bedload transport capacities along the Rhône River, France. Sci. Total Environ. 658, 1375-1389.

https://doi.org/10.1016/j.scitotenv.2018.12.109

Vonwiller, L., Vetsch, D.F., Boes, R.M., 2018. Modeling streambank and artificial gravel deposit erosion for sediment replenishment. Water 10, 1–23. https://doi.org/10.3390/w10040508

Wheaton, J.M., Pasternack, G.B., Merz, J.E., 2004. Spawning habitat rehabilitation-I. Conceptual approach and methods. Int. J. River Basin Manag. 2, 3–20.

Wolman, M.G., 1954. A method of sampling coarse river-bed material. Eos, Trans. Am. Geophys. Union. https://doi.org/10.1029/TR035i006p00951

Zeug, S.C., Sellheim, K., Watry, C., Rook, B., Hannon, J., Zimmerman, J., Cox, D., Merz, J., 2013. Gravel augmentation increases spawning utilization by anadromous salmonids : a case study from california , 718, 707–718. https://doi.org/10.1002/rra

Acknowledgements

This research was supported by the European Regional Development Fund within the project ‘Redynamization of the Old Rhine – 2009–2012’ (FEDER INTERREG IV Upper Rhine; coord. Région Alsace/CNRS UMR 5600 EVS) and by the company Electricité de France (EDF) within the research collaborations ‘Sediment reintroduction into the Old Rhine from controlled bank erosion – 2009–2012’ (EDF 5500-AAH-5910047888), ‘Geomorphic monitoring of gravel augmentation experiment into the Old Rhine – years 2013-2014’ (EDF 5500-4300937910), ‘Redynamization of the Old Rhine – years 2014-2018’ (EDF 5910132058) and by the Région Grand Est (328/14/C1 2016-2017). This work was performed within the framework of the EUR H2O’Lyon (ANR-17-EURE-0018) of the University of Lyon within the program “Investissements d’Avenir” operated by the French National Research Agency (ANR). The authors also warmly thank colleagues who provided fieldwork assistance: J. Houssier, J. Serouilou and G. Skupinski. The authors also want to thank two anonymous reviewers who greatly contributed to improve to this paper by providing helpful reviews of an earlier version of this manuscript.